



Delft University of Technology

Ship energy management for hybrid propulsion and power supply with shore charging

Kalikatzarakis, M.; Geertsma, R. D.; Boonen, E. J.; Visser, K.; Negenborn, R. R.

DOI

[10.1016/j.conengprac.2018.04.009](https://doi.org/10.1016/j.conengprac.2018.04.009)

Publication date

2018

Document Version

Final published version

Published in

Control Engineering Practice

Citation (APA)

Kalikatzarakis, M., Geertsma, R. D., Boonen, E. J., Visser, K., & Negenborn, R. R. (2018). Ship energy management for hybrid propulsion and power supply with shore charging. *Control Engineering Practice*, 76, 133-154. <https://doi.org/10.1016/j.conengprac.2018.04.009>

Important note

To cite this publication, please use the final published version (if applicable).
Please check the document version above.

Copyright

Other than for strictly personal use, it is not permitted to download, forward or distribute the text or part of it, without the consent of the author(s) and/or copyright holder(s), unless the work is under an open content license such as Creative Commons.

Takedown policy

Please contact us and provide details if you believe this document breaches copyrights.
We will remove access to the work immediately and investigate your claim.



Ship energy management for hybrid propulsion and power supply with shore charging



M. Kalikatzarakis ^{a,*}, R.D. Geertsma ^{a,b}, E.J. Boonen ^c, K. Visser ^{a,b}, R.R. Negenborn ^a

^a Department of Maritime & Transport Technology, Delft University of Technology, The Netherlands

^b Faculty of Military Sciences, Netherlands Defence Academy, The Netherlands

^c Damen Shipyards Group, Gorinchem, The Netherlands

ARTICLE INFO

Keywords:

Energy management systems
Propulsion control
Hybrid vehicles
Marine systems
Energy storage
Ship control

ABSTRACT

Hybrid technology in marine vehicles can significantly reduce fuel consumption and local CO₂ emissions. It has been applied successfully to several ship-types, mostly with conventional, rule-based, strategies. To further improve performance, intelligent control strategies are necessary. This work, inspired by automotive research in Energy Management Strategies, applies the Equivalent Consumption Minimisation Strategy (ECMS) to a ship powered by a hybrid propulsion plant with hybrid power supply that can be recharged with renewable shore power. This hybrid configuration has the additional challenge to determine the optimal power-split between three or more different power sources, in real-time, and to optimally deplete the battery packs over the mission profile. To this end, a Mixed-Integer Non-Linear optimisation Problem is formulated and solved by combining Branch & Bound and Convex optimisation. Dynamic Programming (DP) is used to benchmark the real-time strategies, which are also compared to the current rule-based (RB) controller. Simulation results of a case study tugboat with validated models show that, with unknown load demand, 6% additional fuel savings can be achieved with ECMS.

1. Introduction

The shipping sector is responsible for 90% of global freight transportation, which has been increasing by 2.3% annually since 2000 ([Shaheen & Lipman, 2007](#); [Stopford, 2008](#)). Currently, the industry's annual carbon emissions account for more than 3% of the global anthropogenic CO₂ emissions, which could rise up to 8% by 2050 if no CO₂ reduction measures are taken ([International Maritime Organization, 2014](#)). Given these trends, a drastic reduction of fossil fuel usage is practically mandatory. While stationary power consumers can progressively switch to renewable energy sources such as wind energy ([Kumar et al., 2016](#)), tidal energy and solar energy ([Jamel, Rahman, & Shamsuddin, 2013](#)), mobile power consumers often cannot be connected to the electric grid for renewable energy. Moreover, renewable fuels and fuel cells are not available for maritime application in the short term ([Taljegard, Brynolf, Grahn, Andersson, & Johnson, 2014](#); [Van Biert, Godjevac, Visser, & Aravind, 2016](#)). Therefore, the transportation field has to reside to stored energy for its renewable power supply, recharging the energy storage when connected to the main grid. However, only ship types that can connect to the grid regularly, such as ferries, can rely purely on energy storage. Other ship types can use energy storage to reduce

fuel consumption, recharging the energy storage with renewable energy from the grid when moored alongside.

For vessels that experience significant power demand peaks followed by long periods of very low loading, hybrid technology could significantly reduce fuel consumption and emissions. Hybrid technology refers to all plants that consist of (1) hybrid propulsion: a combination of mechanical and electrical propulsion, and (2) hybrid power supply: a combination of combustion power supply and energy storage, found mostly in combination with electric propulsion ([Geertsma, Negenborn, Visser, & Hopman, 2017a](#)). These hybrid propulsion and power supply architectures are capable of reducing fuel consumption and emissions by 10% to 35% according to [Geertsma et al. \(2017a\)](#). However, advanced control strategies are required to regulate power production of all energy sources onboard in order to achieve these savings ([Geertsma et al., 2017a](#); [Grimmelius, de Vos, Krijgsman, & van Deursen, 2011](#); [Herdzik, 2013](#); [Sciberras, Bashar, David, et al., 2015](#); [Shiraishi, Minami, Kobayashi, et al., 2013](#); [Vu, 2015](#); [Vu et al., 2014](#); [Yuan, Tjahjowidodo, Lee, et al., 2016](#); [Zhan, Gao, Chen, & Lin, 2015](#)) and Energy Management strategies are required to make optimum use of

* Correspondence to: Damen Schelde Naval Shipbuilding, Willem Ruysstraat 99, 4381 NK Vlissingen, The Netherlands.
E-mail address: m.kalikatzarakis@damennaval.com (M. Kalikatzarakis).

Nomenclature	
Greek Symbols	
β	hydrodynamic pitch angle in rad
η	efficiency
λ	air excess ratio
λ	air excess ratio
ω	rotational speed in rad/s
ψ	flux linkage in Wb
ρ	density in kg/m ³
θ	angle in rad
Roman Symbols	
c	capacitance in F
c_f	friction factor (fraction of nominal power)
C_Q	propeller torque coefficient
C_T	propeller thrust coefficient
c_{sfo}	specific fuel oil consumption in g/kWh
D	diameter in m
f	frequency in Hz
f_p	power factor
f_w	wake factor
I	Moment of inertia in kg m ²
i	current in A
i_{gb}	gearbox reduction ratio
k_p	number of propellers
L_1	per phase winding inductance in H
M	torque in Nm
m	mass in kg
\dot{m}_f	fuel consumption in kg/s
m_1	trapped mass at the start of compression in kg
m_f	fuel injection per cylinder per cycle in kg
n	rotational speed in Hz
P	power in W
p_1	charge air pressure in Pa
p_6	average pressure in the cylinder during exhaust opening in Pa
p_{\max}	maximum pressure during combustion in the Seiliger cycle in Pa
p_p	pole pairs
p_d	pressure in the exhaust receiver in Pa
Q	heat in J
Q_{bat}	battery capacity in Ah
Q_{lhv}	lower heating value of fuel at ISO conditions in kJ/kg
q_{23}	specific heat release at constant volume in kJ/kg
q_{34}	specific heat release at constant pressure in kJ/kg
q_{45}	specific heat release at constant temperature in kJ/kg
R	ship resistance in N
r	resistance in Ohm
s	equivalence factor
s_l	slip
S_{OC}	state of charge
T	thrust in N
t	time in sec
T_6	average temperature in the cylinder during exhaust opening in K
t_p	thrust reduction factor
u	voltage in V
u_c	control variables for the control problem
v_a	advance velocity in m/s
v_s	ship speed in m/s
w_i	specific indicated work during the Seiliger cycle in kNm/kg
w_e	exogenous inputs for the control problem
X_{tow}	tow force in N
Superscripts	
*	normalised values
Subscripts	
aux	demand for auxiliary loads
b	base
bat	battery
chg	charge
d	direct axis in dq reference frame
dg	diesel generator
dis	discharge
el	electric
eqv	equivalent
fc	frequency converter
g	synchronous generator
gb	gearbox
i	core branch
im	induction machine
line	network line
loss	losses
m	mutual
me	main engine
mmf	stator magnetic field
nom	nominal
oc	open cell
p	propeller
pd	demand for propulsion
q	quadrature axis in dq reference frame
r	rotor
rec	rectifier
rr	relative rotative
s	stator
set	setpoint
sh	shaft
sl	slip
sync	synchronous
t	terminal
th	thruster
tot	total

batteries over time and thus reduce fuel consumption and emissions (Sciarretta, Back, & Guzzella, 2004; Vu, 2015; Vu et al., 2014).

1.1. Literature review

Hybrid propulsion is typically applied to naval vessels (Castles, Reed, Bendre, & Pitsch, 2009; Geertsma, Negenborn, Visser, & Hopman, 2016; Sulligoi et al., 2012), towing vessels (Wijsmuller M., 2007), offshore vessels (Barcellos, 2013; Herdzik, 2013), research vessels (Capasso et al., 2016) and yachts (van Loon & van Zon, 2016). These applications all feature an operating profile with a significant period of time at high speed and power and a significant period of time at low speed and propulsion power. The mechanical propulsion plant provides very efficient high speed operation and the electrical propulsion plant provides efficient and potentially very silent low speed operation due to the power station concept (Geertsma et al., 2017a; Veneri, Migliardini, Capasso, & Corbo, 2012).

Hybrid power supply has recently become a realistic option for many maritime applications due to the development of power dense lithium-ion battery technologies, developed for the automotive industry. As argued in Capasso and Veneri (2014), lithium-ion batteries provide power and energy dense energy storage with good life cycle performance

and have thus enabled electrical, hybrid and plug-in hybrid vehicles in the automotive market. Particularly, lithium-ion polymer batteries and lithium iron phosphate batteries provide high capacity at high discharge currents. Capasso and Veneri (2014) reported experimental analysis that demonstrated the excellent performance of lithium iron phosphate batteries during high discharge current, and excellent charging efficiency of lithium-ion polymer batteries. These characteristics of lithium iron phosphate batteries and their thermal stability and relative safety have led to their applications in hybrid tugs (de Groote & van Koperen, 2014).

Thus, hybrid power supply has been applied to towing vessels (Brejts & El Aman, 2016; Drijver, 2013; van Koperen, 2009; Volker, 2013), yachts (Bosich & G.Sulligoi, 2013; Dedes, Hudson, & Turnock, 2012; Grimmelius et al., 2011), ferries (Ovrum & Bergh, 2015; Veneri et al., 2012; Zahedi, Norum, & Ludvigsen, 2014), research (Capasso et al., 2016), naval (Doerry, Robey, Amy, & Petry, 1996; Whitelegg, Bucknall, & Thorp, 2015), and offshore vessels (Zahedi & Norum, 2013). In these applications the total electrical load varies significantly over time and in some cases has steep power increases and decreases. Therefore, the use of energy storage, such as batteries and super capacitors, can provide peak shaving, load levelling, frequency control and improving quality of power supply, and enable switching off all engines to reduce noise for a limited period (Dedes et al., 2012; Falcao, Castro, & de Jesus, 2016; Whitelegg et al., 2015; Zahedi et al., 2014). Moreover, the batteries can be recharged from the shore grid, when the ship is moored alongside, reducing local emissions (Brejts & El Aman, 2016; Geertsma et al., 2017a). Finally, the batteries can provide back-up power during failures of diesel generators, negating the need for spinning reserve (Zahedi et al., 2014).

Advanced control in land-based hybrid electric vehicles has been a field of extensive research for almost twenty years (Ambuhl, Sundstrom, Sciarretta, & Guzzella, 2010; Baumann, Rizzoni, & Washington, 1998; Chasse & Sciarretta, 2011; Dib, Chasse, Moulin, Sciarretta, & Corde, 2014; Formentin, Guanetti, & Savaresi, 2016; Guzzella, Sciarretta, et al., 2007; Johannesson, Murgovski, Jonasson, Hellgren, & Egardt, 2015; Kermani, Delprat, Guerra, Trigui, & Jeanneret, 2012; Koot et al., 2005; Nuesch et al., 2014; Paganelli et al., 2000; Salman, Schouten, & Kheir, 2000; Sciarretta et al., 2004). For the automotive field, comparative studies have demonstrated that an optimal control-based approach can outperform rule-based approaches (Sciarretta et al., 2014). In particular, Sciarretta et al. (2014) demonstrated that various implementations of the Equivalent Consumption Minimisation Strategy (ECMS) can approximate the fuel economy of acausal controllers, with low computational burden and limited calibration of control parameters. While initial research in this field focussed on charge sustaining strategies, the rise of Plug-in Hybrid Electric Vehicles (PHEV) has stimulated research into charge depleting ECMS strategies. The aim of such a charge depleting ECMS is to generate an optimal discharge trajectory for the battery (Guardiola, Pla, Onori, & Rizzoni, 2014). Ideally, progressive battery discharge, *blended-mode*, will be the output of the EMS, as the repetitive sequence of electrical charge depleting operation followed by charge sustaining operation is known to be far from optimal from a fuel economy standpoint (Guardiola et al., 2014; Sciarretta et al., 2014).

Energy management strategies, such as ECMS, can also reduce fuel consumption and emissions on ships with electric propulsion and hybrid power supply (Brejts & El Aman, 2016; Haseltalab, Negenborn, & Lodewijks, 2016; Vu, 2015; Yuan et al., 2016). First, Vu (2015) concludes that an ECMS strategy with a novel operating load estimation scheme on an electric tug with diesel electric propulsion and hybrid power supply can save up to 9% fuel, compared to the rule-based controller described in Sciberras and Norman (2012). However, the robustness of the estimation scheme against varying operating profiles is not investigated. Similarly, Yuan et al. (2016) report 17% savings for a similar tug with ECMS without knowledge or prediction of the future, compared to a charge-sustaining rule-based strategy. They both recognise that fuel economy is mainly attributed to the charge-depleting

nature of ECMS rather than to its ability to identify more efficient operating modes for the propulsion plant. Haseltalab et al. (2016) demonstrate how multi-level Model Predictive Control can handle environmental disturbances and ship model uncertainties with a case study offshore vessel with electric propulsion and hybrid power supply. A comparative analysis with a conventional control solution is not documented. Brejts and El Aman (2016) establish the optimum power split for the hybrid power supply of a ferry with electric propulsion with a combination of a rule-based strategy for discrete decisions and ECMS. They report an additional 11% fuel consumption reduction due to their ECMS framework during actual sea trials.

None of the studies discussed above compares the results with a causal, optimum, controller, or addresses the robustness of its solution to a change in the operating profile. Research into hybrid propulsion with ECMS is even more limited: Grimmelius et al. (2011) demonstrate the feasibility of ECMS for hybrid propulsion with a simulation study, however they only utilise energy storage for electric power supply, use an inaccurate linear problem formulation, and lack a comparative analysis with a conventional control strategy.

1.2. Aim and contribution

In this paper, we investigate how much fuel consumption and local CO₂ emission reduction can be achieved by applying ECMS to a hybrid propulsion plant with hybrid power supply with and without future operating load estimation, and determine the robustness of the ECMS performance against varying operating profiles compared to the global optimum solution with a priori knowledge and determined with DP. We use a case study towing vessel with hybrid propulsion plant and hybrid power supply, as shown in Fig. 2.

The novelty of this work is threefold. First, we propose a simulation model that uses an improved version of the Mean Value First Principle diesel engine model proposed in Geertsma, Negenborn, Visser, and Hopman (2017b), to reflect the effect of mean effective pressure on mechanical efficiency and the effect of air excess ratio and peak combustion pressure on heat loss. The resulting propulsion system model has been validated with measurements and manufacturer data, on top of the propulsion model validation reported in Geertsma et al. (2017b). Second, a novel approach is proposed for the on-line solution of the charge depleting ECMS control problem with discrete variables for the various engines and operating modes, by splitting the problem formulation in convex sub-problems, and combining branch and bound with convex optimisation. This approach is applied to an ECMS approach without and with operator load estimation. Third, the optimality and robustness of the two proposed strategies are compared with a rule-based strategy as applied on the tug in Fig. 2 and the global optimum from Dynamic Programming (DP), assuming apriori knowledge on the operating profile.

1.3. Outline

This paper is organised as follows: Section 2 describes the system and presents the modelling approach, and Section 3 discusses the ECMS and causal control strategies, their control objectives and solution. The results of the comparison between the existing rule-based controller, the ECMS strategies and the causal controller are presented in Section 4. Finally, Section 5 summarises the conclusions of this study and provides suggestions for further work.

2. System description & modelling

In this study, we consider hybrid propulsion with hybrid power supply for ships. The propulsion system of the case study tug, shown in Fig. 1, consists of two thrusters with fixed pitch propellers, two high-speed 4-stroke diesel engines with a combined power of 3680 kW (4935 hp) at 1600 rpm, two induction machines of 230 kW each and two



Fig. 1. Damen Azimuth Stern Drive 2810 Hybrid Tugboat, case study in this paper.

lithium iron magnesium phosphate battery packs of 120 kWh each, as shown in Fig. 2 and described in de Groot and van Koperen (2014). The main engines can propel the vessel up to 13 knots, with a maximum bollard pull of 60 tons.

The model of the hybrid propulsion and power generation plant and its control is illustrated in Fig. 4 and uses the modular, hierarchical and causal modelling approach, as discussed in Colonna and Van Putten (2007). While this dynamic approach is not required for accurate fuel consumption estimation, it allows to investigate other measures of performance such as engine thermal loading, manoeuvrability and cavitation noise as discussed in Geertsma et al. (2017b) and Geertsma, Vollbrandt, Negenborn, Visser, and Hopman (2017). In this study, we therefore use the dynamic simulation model as the benchmark system against which we establish the fuel economy performance of the various considered Energy Management strategies. The models of the mechanical propulsion plant, consisting of the main diesel engine (ME), governor (GOV), transmission (TRM), and propeller (PROP), are based on the validated Mean Value First Principle models of Geertsma et al. (2017b). Improvements on the diesel engine model, and the models of the transmission, propeller, hull, induction machine (IM), batteries (BAT) and diesel generator (DG) sets will be discussed below.

The operating profile of a tug is determined by the vessel speed v_s and the towing force, X_{tow} . The operating profile synthesis determines the speed setpoint for the model with a PI control loop. The energy management strategy proposed in Section 3 of this study subsequently determines the following control setpoints: speed setting of the main engines (MEs) $n_{\text{me},\text{set}}$, speed or torque setting of the Induction Machines (IMs) $n_{\text{im},\text{set}}$ or $M_{\text{im},\text{set}}$ and current setting of the Battery (BAT) $i_{\text{bat},\text{set}}$.

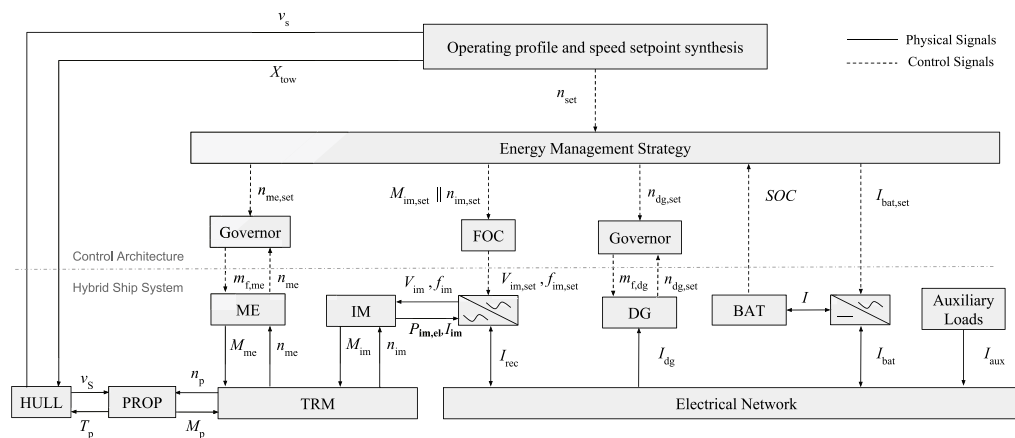


Fig. 4. Schematic presentation & causality graph of the simulation model (propulsion and control system) showing coupling between models.

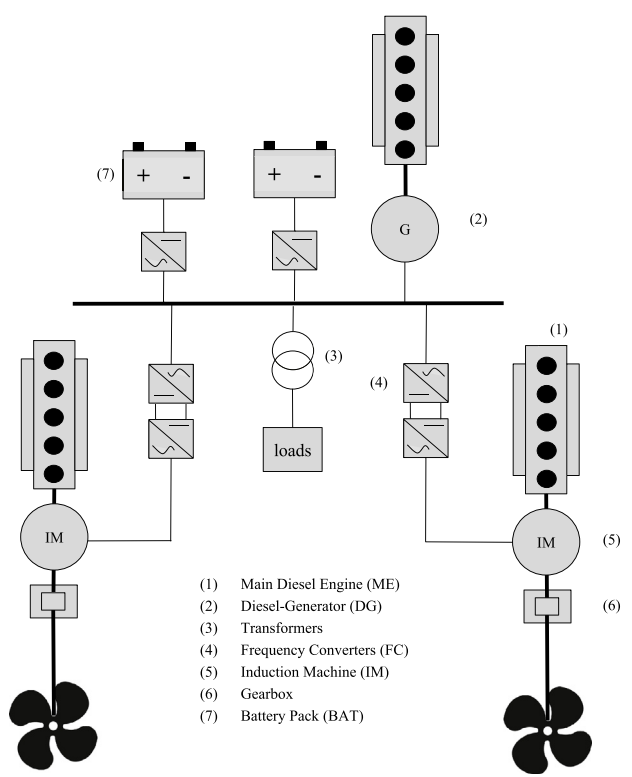


Fig. 2. Hybrid propulsion with hybrid power supply, case study in this paper.

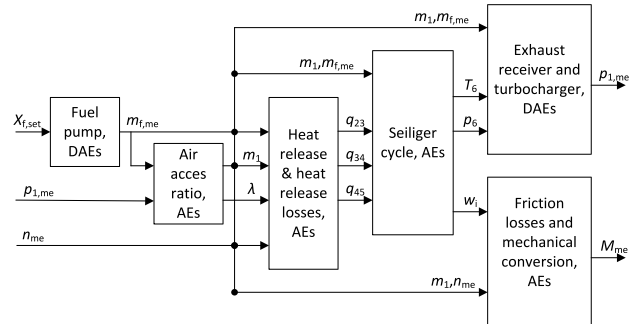


Fig. 3. Schematic presentation of the diesel engine model and the interaction between its subsystems, consisting of Algebraic Equations (AE) or Differential and Algebraic Equations (DAE).

2.1. Diesel engine and governor

For the main diesel engines (MEs), we use the Mean Value First Principle model proposed and validated with Factory Acceptance Test (FAT) and Sea Acceptance Trial (SAT) data in Geertsma et al. (2017b). Fuel consumption of the main engines, for a given engine torque or load, depends on engine speed and charge pressure, as illustrated in Fig. 3. The full equations of the model are covered in Geertsma et al. (2017b). In summary, engine fuel consumption is mainly determined by the mathematical relationship between engine torque M_{me} and engine fuel injection pump position $X_{\text{f, set}}$, charge air pressure $p_{1,\text{me}}$, and engine speed n_{me} , while the turbocharger dynamics govern engine charge pressure p_1 . The schematic presentation in Fig. 3 provides the interaction between the engine model subsystems and the governing equations as described in Geertsma et al. (2017b). The summarising equations are as follows:

$$\frac{dm_{\text{f,me}}(t)}{dt} = f_1(X_{\text{f, set}}(t), m_{\text{f,me}}(t)) \quad (1)$$

$$m_1(t) = f_2(m_{\text{f,me}}(t), p_{1,\text{me}}(t), n_{\text{me}}(t)) \quad (2)$$

$$\lambda(t) = f_3(m_{\text{f,me}}(t), p_{1,\text{me}}(t), n_{\text{me}}(t)) \quad (3)$$

$$q_{23}(t) = f_4(m_{\text{f,me}}(t), p_{1,\text{me}}(t), n_{\text{me}}(t)) \quad (4)$$

$$q_{34}(t) = f_5(m_{\text{f,me}}(t), p_{1,\text{me}}(t), n_{\text{me}}(t)) \quad (5)$$

$$q_{45}(t) = f_6(m_{\text{f,me}}(t), p_{1,\text{me}}(t), n_{\text{me}}(t)) \quad (6)$$

$$T_6(t) = f_7(m_{\text{f,me}}(t), m_1(t), q_{23}(t), q_{34}(t), q_{45}(t)) \quad (7)$$

$$p_6(t) = f_8(m_{\text{f,me}}(t), m_1(t), q_{23}(t), q_{34}(t), q_{45}(t)) \quad (8)$$

$$w_i(t) = f_9(m_{\text{f,me}}(t), m_1(t), q_{23}(t), q_{34}(t), q_{45}(t)) \quad (9)$$

$$\frac{dp_d(t)}{dt} = f_{10}(m_{\text{f,me}}(t), m_1(t), T_6(t), p_6(t)) \quad (10)$$

$$\frac{dp_{1,\text{me}}(t)}{dt} = f_{11}(m_{\text{f,me}}(t), m_1(t), T_6(t), p_d(t)) \quad (11)$$

$$M_{\text{me}}(t) = f_{12}(w_i(t), m_1(t), n_{\text{me}}(t)). \quad (12)$$

While for the specific engine in the case study the accuracy of this model at very low loads is insufficient to determine optimal energy management, the accuracy of fuel consumption prediction has been improved with two amendments to the model, as discussed below.

2.1.1. Mechanical losses

Chen and Flynn (1965) have experimentally established that mechanical losses due to friction M_{loss} in Nm can be derived from mean piston speed and mean effective pressure. By correlating (1) the mean piston speed with the rotational speed of the shaft n_{me} in Hz, and (2) the mean effective pressure with the maximum pressure of the Seiliger process p_{max} in Pa, friction losses can be estimated as follows¹:

$$M_{\text{loss}}^*(t) = a + bp_{\text{max}}^*(t) + cn_{\text{me}}^*(t) + dn_{\text{me}}^{*2}(t), \quad (13)$$

with $a, b, c, d \in (0, 1)$ fitted parameters that can be calibrated with manufacturer data.

2.1.2. Cylinder heat losses

Heywood et al. (1988) argue that several variables affect the magnitude of heat lost to the combustion chamber surfaces \bar{Q}_{loss}^* in J. The most important are engine speed, load and air excess ratio λ . After a thermodynamic analysis based on (Stapersma, 2010a, b, c, d), the following relation was derived (Kalikatzarakis, 2017):

$$\bar{Q}_{\text{loss}}^*(t) = w_1 \left(-\frac{c_1}{\lambda^{*2}(t)} + 2\frac{c_1}{\lambda^*(t)} + c_2 \right) + w_2 \frac{p_{\text{max}}^{*0.7}(t)}{n_{\text{me}}^{*0.3}(t)}, \quad (14)$$

with $c_1, c_2 \in (0, 1)$ $w_1, w_2 \in (0, 1)$, $\sum_{i=1}^2 w_i = 1$, fitted parameters that can be calibrated with manufacturer data.

¹ The superscript * denotes normalised values.

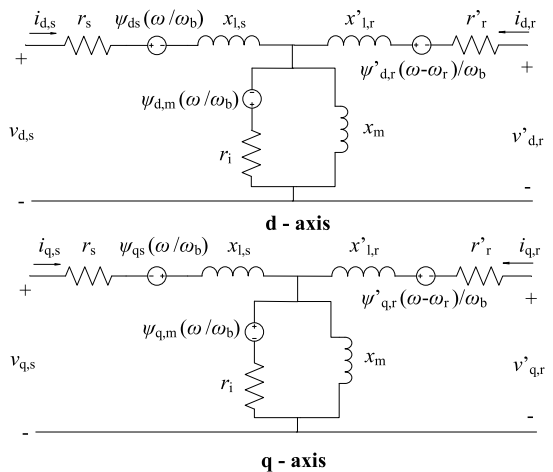


Fig. 5. Dq equivalent circuit of an induction machine in an arbitrary rotating reference frame.

2.2. Induction machine and frequency converter

For the induction machines, a state space model based on (Khoury, Ghosn, Khatounian, Fadel, & Tientcheu, 2016; Ong, 1998) is used, shown in Fig. 5. The zero sequence voltage and current have been neglected, as electrical faults causing asymmetries in the phase impedances are outside the scope of this work. The resulting voltage u_{dq} in V, flux linkage ψ_{dq} in Wb, in the dq reference frame, and torque equations M_{im} in Nm are given below.

Stator and rotor voltage equations:

$$u_{q,s}(t) = \frac{d}{dt} \frac{\psi_{q,s}(t)}{\omega_b} + r_s i_{q,s}(t) + \omega_{\text{mmf}}(t) \frac{\psi_{d,s}(t)}{\omega_b} \quad (15)$$

$$u_{d,s}(t) = \frac{d}{dt} \frac{\psi_{d,s}(t)}{\omega_b} + r_s i_{d,s}(t) + \omega_{\text{mmf}}(t) \frac{\psi_{q,s}(t)}{\omega_b} \quad (16)$$

$$u_{q,r}(t) = 0 = \frac{d}{dt} \frac{\psi'_{q,r}(t)}{\omega_b} + (\omega_{\text{mmf}}(t) - \omega_{\text{im}}(t)) \frac{\psi'_{d,r}(t)}{\omega_b} + r'_r(t) i'_{q,r}(t) \quad (17)$$

$$u_{d,r}(t) = 0 = \frac{d}{dt} \frac{\psi'_{d,r}(t)}{\omega_b} - (\omega_{\text{mmf}}(t) - \omega_{\text{im}}(t)) \frac{\psi'_{q,r}(t)}{\omega_b} + r'_r(t) i'_{d,r}(t). \quad (18)$$

Magnetic branch equations:

$$r_i i_{q,i}(t) = \frac{d}{dt} \frac{\psi_{q,m}(t)}{\omega_b} + \omega_{\text{mmf}}(t) \frac{\psi_{q,m}(t)}{\omega_b} \quad (19)$$

$$r_i i_{d,i}(t) = \frac{d}{dt} \frac{\psi_{d,m}(t)}{\omega_b} + \omega_{\text{mmf}}(t) \frac{\psi_{d,m}(t)}{\omega_b}. \quad (20)$$

Stator and rotor flux linkages:

$$\frac{\psi_{q,s}(t)}{\omega_b} = \frac{\psi_{q,m}(t)}{\omega_b} + L_{l,s} i_{q,s}(t) \quad (21)$$

$$\frac{\psi_{d,s}(t)}{\omega_b} = \frac{\psi_{d,m}(t)}{\omega_b} + L_{l,s} i_{d,s}(t) \quad (22)$$

$$\frac{\psi'_{q,r}(t)}{\omega_b} = \frac{\psi_{q,m}(t)}{\omega_b} + L'_{l,r} i'_{q,r}(t) \quad (23)$$

$$\frac{\psi'_{d,r}(t)}{\omega_b} = \frac{\psi_{d,m}(t)}{\omega_b} + L'_{l,r} i'_{d,r}(t). \quad (24)$$

Mutual flux linkages:

$$\frac{\psi_{d,m}(t)}{\omega_b} = L_m i_{d,m}(t) \quad (25)$$

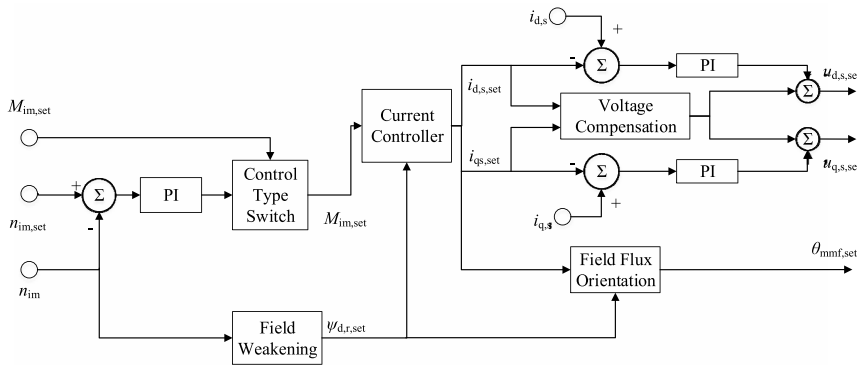


Fig. 6. Schematic representation of Field Oriented Control.

$$\frac{\psi_{q,m}(t)}{\omega_b} = L_m i_{q,m}(t). \quad (26)$$

Current equations:

$$i_{d,s}(t) + i'_{d,r}(t) = i_{d,m}(t) + i_{d,i}(t) \quad (27)$$

$$i_{q,s}(t) + i'_{q,r}(t) = i_{q,m}(t) + i_{q,i}(t). \quad (28)$$

Synchronous speed and slip:

$$\omega_{sync}(t) = \frac{2}{p_p} \omega_{mmf}(t) \quad (29)$$

$$n_{sl}(t) = \frac{60 \omega_{sync}(t)}{2\pi} = \frac{120 f_{mmf}(t)}{p_p} \quad (30)$$

$$s_1(t) = \frac{\omega_{sync}(t) - \omega_{im}(t)}{\omega_{sync}(t)}. \quad (31)$$

Torque equation:

$$M_{im}(t) = \frac{3}{2\omega_b} \frac{p_p}{2} \times (\psi_{d,r}(t) (i_{q,s}(t) - i_{q,i}(t)) - \psi_{q,r}(t) (i_{d,s}(t) - i_{d,i}(t))). \quad (32)$$

For primary control of the IMs, Field Oriented Control (FOC) is used (Trzynadlowski, 2001), according to the diagram in Fig. 6. The actual IM speed n_{im} is compared to the IM speed set-point $n_{im, set}$, and converted to a torque setting $M_{im, set}$ by means of a PI-controller. The control type switch changes between torque and speed control, depending on the state of the main engines. Either the main engines run in speed control and the electric machines in torque control or the engines are switched off and the electric machines run in speed control. Field weakening determines the direct component of the flux vector, which depends on shaft speed. For speeds lower than the rated speed of the IM, the flux is set at its rated value, while for higher speeds flux reduction is proportional to speed increase, to maintain maximum voltage and constant power (Ong, 1998). The current controller determines the stator dq-current vector in A, as a function of the torque setting and the flux d-component:

$$i_{q,s, set}(t) = \frac{M_{im, set}(t)}{\frac{3}{2} \frac{p_p}{2} \frac{L_m}{L'_{lr} + L_m} \frac{\psi_{d,r}(t)}{\omega_b}} + i_{q,i}(t) \quad (33)$$

$$i_{d,s, set}(t) = \frac{\psi_{d,r}(t)}{\omega_b} (r_r + (L'_{lr} + L_m)) \frac{1}{r_r L_m} + i_{d,i}(t). \quad (34)$$

The current vector is then converted to the dq-voltage vector by means of PI-controllers, to which two extra feed-forward terms are added [$u_{d,s, set, FF}$, $u_{q,s, set, FF}$] for voltage compensation and to increase the performance of the control scheme (Ong, 1998):

$$u_{d,s, set, FF}(t) = \frac{L_m^2}{L'_{lr} + L_m} \frac{d}{dt} i_{d,s, set}(t) - \omega_{mmf}(t) \frac{L'_{lr}}{L_m} (L_{ls} + L_m) i_{q,s, set}(t) \quad (35)$$

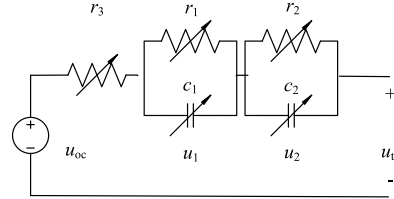


Fig. 7. Battery equivalent circuit.

$$u_{d,s, set, FF}(t) = \omega_{mmf}(t) \frac{L'_{lr}}{L_m} (L_{ls} + L_m) i_{d,s, set}(t) + \frac{L_m^2}{L'_{lr} + L_m} \frac{d}{dt} i_{q,s, set}(t). \quad (36)$$

The field flux orientation block determines the slip speed and desired flux angle θ_{mmf} , with respect to the set-points of the quadrature component of the current vector, and the direct component of the flux vector, as follows:

$$\omega_{sl}(t) = r'_r \frac{L_m}{L'_{lr} + L_m} \frac{i_{q,s, set}(t) - i_{q,i}(t)}{\frac{\psi_{d,r, set}(t)}{\omega_b}} \quad (37)$$

$$\frac{d\theta_{mmf}(t)}{dt} = \omega_{mmf}(t) = (\omega_{im}(t) + \omega_{sl}(t)). \quad (38)$$

Finally, the power losses of the frequency converter (FC) are estimated using the empirical relation of Ross, Stapersma, and Bosklopper (2010), leading to the converter power on the network side P_{fc} , as follows:

$$P_{fc, loss}(t) = P_{fc, nom}(1 - \eta_{fc, nom}) (a + b i_{fc}^*(t) + c i_{fc}^{*2}(t)) \quad (39)$$

$$P_{fc}(t) = P_{im, el} + P_{fc, loss}, \quad (40)$$

with $a, b, c \in (0, 1)$ fitted parameters.

2.3. Battery

The battery model is used to evaluate the battery dynamics and in particular the relationship between the open cell voltage and the state of charge (SOC). Although in this study we assume the state of charge feedback to the Energy Management Strategy is accurate, the used battery model could also be used to investigate SOC estimation schemes and the impact of inaccurate SOC estimation on EMS performance. Therefore, the battery is represented by a 2nd order electrical equivalent circuit model, given in Fig. 7, as proposed in Tian, Xia, Wang, Sun, and Xu (2014). Equivalent circuit models with one resistor and two resistor-capacitor elements provide a good trade-off between model complexity and accuracy in describing voltage dynamics of a lithium-ion battery (Hu, Li, & Peng, 2012; Tian et al., 2014). In the proposed model, the open circuit voltage (u_{oc}) in V, capacitors (c_i) in F and resistors (r_i)

in Ohm, are functions of the state of charge (SOC), as follows (Erdinc, Vural, & Uzunoglu, 2009; Gao, Liu, & Dougal, 2002):

$$u_{oc}(S_{OC}(t)) = v_1 e^{-v_2 S_{OC}(t)} + v_3 + v_4 S_{OC}(t) + v_5 S_{OC}^2(t) + v_6 S_{OC}^3(t) \quad (41)$$

$$r_i(S_{OC}(t)) = \alpha_{i,1} e^{-\alpha_{i,2} S_{OC}(t)} + \alpha_{i,2}, \quad i = 1, 2 \quad (42)$$

$$c_i(S_{OC}(t)) = \beta_{i,1} e^{-\beta_{i,2} S_{OC}(t)} + \beta_{i,2}, \quad i = 1, 2. \quad (43)$$

The constants $\vec{v} = (v_1, \dots, v_6) \in \mathbb{R}^6$ and arrays $\mathbf{A} = (\alpha_{i,j}) \in \mathbb{R}^{3 \times 2}$, $\mathbf{B} = (\beta_{i,j}) \in \mathbb{R}^{2 \times 2}$ constitute the model's parameters.

The circuit behaviour is described as follows:

$$\frac{d}{dt} u_i(t) = -\frac{u_i(t)}{c_i r_i} + \frac{i_{bat}(t)}{c_i}, \quad i = 1, 2 \quad (44)$$

$$u_i(t) = u_{oc}(t) - \sum_{i=1}^2 u_i(t) - r_3 i_{bat}(t). \quad (45)$$

The performance of any energy management strategy strongly depends on accurate SOC estimation, because the use of the battery is constrained by a minimum SOC to limit battery degradation, and adaptive strategies adapt the use of the battery as a function of the SOC. However, accurate SOC estimation remains challenging, because SOC cannot be directly measured and is influenced by parameters such as battery temperature and battery ageing (Hu et al., 2012; Tian et al., 2014; Waag, Fleischer, & Sauer, 2014). While the Ampere-hour (Ah) counting method is the simplest method, it is susceptible to accumulated SOC drift due to current measurement errors and requires recalibration with other methods, such as estimation based on open cell voltage (OCV) (Zheng et al., 2016) or model based estimation (Tian et al., 2014). A comprehensive review of SOC estimation techniques and other battery management system functions is available in Waag et al. (2014). For this study, we neglect measurement inaccuracies and therefore use Ah counting to estimate SOC, as follows:

$$S_{OC}(t) = S_{OC}(t_0) + \int_{t_0}^t -\frac{i_{bat}(t)}{Q_{bat}} dt. \quad (46)$$

2.4. Auxiliary loads

The electrical network needs to supply the load for the frequency converters for the induction machines (IMs) when in motoring mode, the battery when in charging mode and all auxiliary electrical loads. While these auxiliary loads fluctuate during tug operations, in this study we do not consider the effect of the auxiliary load and consider this load constant. The relationship between the auxiliary load power P_{aux} and the auxiliary current i_{aux} for the three phase electrical network is defined as follows:

$$P_{aux}(t) = 3u_g(t)i_{aux}(t) \cos(f_p). \quad (47)$$

2.5. Diesel-generator set

This study does not consider the electrical network dynamics since they do not influence fuel consumption (Patel, 2012). As such, simplified models have been developed for the components of the diesel-generator (DG) set, which assume constant voltage and allow us to omit the Automatic Voltage Generator (AVR). A PI controller represents the governor of the DG, and a quadratic relation between torque and injected fuel per cycle has been assumed for the DG, as proposed in Shi, Grimmelius and Stapersma (2010) and omitting the dependency on engine speed as the DG runs at constant speed. A steady-state model, based on the per-phase equivalent circuit of Fig. 8 has been used for the synchronous generator. Its state is estimated from the required network current, which is converted into torque demand towards the DG.

First, the instantaneous per-phase voltage u_g , is derived as follows:

$$u_{g,nom}(t) = \frac{u_{line}(t)}{\sqrt{3}} \quad (48)$$

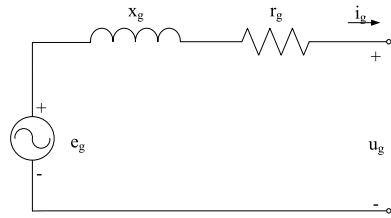


Fig. 8. Synchronous generator per-phase equivalent circuit.

$$\omega_{g,el,nom}(t) = \omega_{dg,nom}(t) \frac{p_p}{2} \quad (49)$$

$$u_g(t) = u_{g,nom}(t) \frac{\omega_{g,el}(t)}{\omega_{el,nom}(t)} = u_{g,nom}(t) \frac{\omega_{dg}(t)}{\omega_{dg,nom}(t)}. \quad (50)$$

Subsequently, power input to the generator P_g and electrical power to the network P_{el} in W are determined as follows:

$$P_{g,el}(t) = 3u_g(t)i_g(t) \cos(f_p) \quad (51)$$

$$P_{g,loss}(t) = \underbrace{P_{g,nom} c_f}_{\text{Friction Losses}} + \underbrace{|i_g(t)|^2 r_g}_{\text{Copper Losses}} \quad (52)$$

$$P_g(t) = P_{g,el}(t) + P_{g,loss}(t) \quad (53)$$

$$M_g(t) = \frac{P_g(t)}{\omega_{dg}(t)}. \quad (54)$$

Finally, the generator dynamics balancing power provided by the generator diesel P_{dg} and power provided to the generator P_g , and the speed governor are represented as follows:

$$m_{f,dg}(t) = K_P \left(\omega_{dg,sett}^* - \omega_{dg}(t)^* \right) + \quad (55)$$

$$K_I \int_0^t \left(\omega_{dg,sett}^* - \omega_{dg}(t)^* \right) dt \quad (56)$$

$$M_{dg}^* = (1 - a(1 - m_f^*) + b(1 - m_f^*)^2) \quad (56)$$

$$\frac{d\omega_{dg}}{dt} = \frac{M_{dg} - M_g}{2\pi I_{dg}}, \quad (57)$$

with $a, b, c \in (0, 1)$ fitted parameters.

2.6. Propeller

The goal of the propeller model is to predict thrust and torque characteristics as a function of propeller speed. To this end, the 4-quadrant open water diagram has been used, based on the Wageningen B data series of the Maritime Research Institute Netherlands (MARIN) (Kuijer, 1992). These describe the relationship between the hydrodynamic pitch angle β and the propeller torque and thrust coefficients (C_T^* , C_Q^*). Subsequently, propeller thrust T_p in N and torque M_p in Nm can be established via the torque and thrust coefficients (C_T , C_Q) respectively, as follows:

$$\beta(t) = \arctan \left(\frac{v_a(t)}{0.7\pi n_p(t) D_p} \right) \quad (58)$$

$$v_a(t) = (1 - f_w) v_s(t) \quad (59)$$

$$T_p(t) = \frac{C_T(t)(1 - t_p)}{\frac{1}{2}\rho(v_a^2(t) + (0.7\pi n_p(t) D_p)^2) \frac{\pi}{4} D_p^2} \quad (60)$$

$$M_p(t) = \frac{C_Q(t)}{\frac{1}{2}\rho\eta_{rr}(v_a^2(t) + (0.7\pi n_p(t) D_p)^2) \frac{\pi}{4} D_p^3}. \quad (61)$$

2.7. Gearbox and shaft-line

The gearbox and shaft line model predicts the losses in the gearbox and accounts for the speed reduction of the gearbox. Godjevac, Drijver,

de Vries, and Stapersma (2015) has demonstrated that a properly calibrated empirical gearbox loss model can accurately match the prediction of a thermal loss model, for which often insufficient date is available. We have used the quadratic empirical model proposed in Drijver (2013) and Godjevac et al. (2015), as follows:

$$M_{gb,loss}^*(t) = a + b n_p^*(t) + c n_p^{*2}(t) + d \frac{(M_{im} + M_{me})}{(M_{im,nom} + M_{me,nom})}, \quad (62)$$

with $a, b, c, d \in (0, 1)$ fitted parameters.

The equation of motion for the prime movers, shaft-line, gearbox and propeller, which are assumed to be rigidly coupled (Geertsma et al., 2017b), is represented as follows:

$$\frac{dn_p(t)}{dt} = \frac{1}{2\pi} \frac{i(M_{im}(t) + M_{me}(t)) - M_{gb,loss} - M_p(t)}{I_{tot}(t)} dt. \quad (63)$$

2.8. Hull dynamics

This study analyses ship motion only in the surge direction, thus the hull model needs to provide an estimate of the vessel's resistance R in N, as a function of its speed v_s . The resistance curve is derived from sea trials, and the propeller-hull interaction coefficients have been established from practical estimations. The equation of motion represents the ship's manoeuvring dynamics in one degree of freedom, similar to the validated approach of Geertsma et al. (2017b).

$$\frac{dv_s(t)}{dt} = \frac{1}{m} \left(k_p T_p(t) \cos(\theta_{th}(t)) - \frac{R(v_s(t))}{1-t} - X_{tow}(t) \right) \quad (64)$$

2.9. Model summary

In summary, the hybrid ship system model consists of 5 sub-models with a system of Differential and Algebraic Equations (DAEs) and 2 sub-models consisting of Algebraic Equations (AE) with the relations shown in Fig. 4. The diesel engine model, a system of DAEs, consists of the state variables fuel injection per cylinder per cycle m_f , charge pressure p_1 and exhaust receiver pressure p_d . The induction machine and frequency converter model is a system of DAEs with 6 state variables for the direct and quadrature flux linkages of the stator, the rotor and the mutual flux $\Psi_{q,s}$, $\Psi_{d,s}$, $\Psi_{q,r}$, $\Psi_{d,r}$, $\Psi_{d,m}$ and $\Psi_{q,m}$, and the DAEs of the battery model consist of state variables terminal voltage u_t and battery state of charge S_{OC} . The gearbox and shaft-line model contains DAEs with state variable propeller speed n_p and the hull is a system of DAEs with state variable ship speed v_s . The diesel generator model consist of a system of DAEs with state variable diesel generator speed n_{dg} . Finally, the propeller model consist of a system of AE's.

The primary control strategies of the propulsion plant are included in the model as the ECMS strategies investigated in this work are aimed at the secondary energy management, as indicated in Fig. 4. The primary control strategy consist of speed control for the main diesel engine and diesel generator set controlling the control variable fuel injection setpoint $m_{f,me,set}$ for the main diesel engine and the variable fuel injection for the diesel generator $m_{f,dg,set}$, based on engine speed feedback. The primary control strategy of the IM consists of Field Oriented Control, controlling the control variables voltage and frequency V_{fc} and f_{fc} for the frequency converter, based on induction machine speed and current feedback. The resulting current subsequently has a mathematical relationship with the generator and battery current.

2.10. Model calibration and validation

2.10.1. Diesel engine and governor

The parameters used in the diesel engine model have been obtained from three different sources. Most of the parameters are available from the manufacturer, and several have been estimated based on FAT data and diesel engine or general physics theory (Stapersma, 2010a, b,

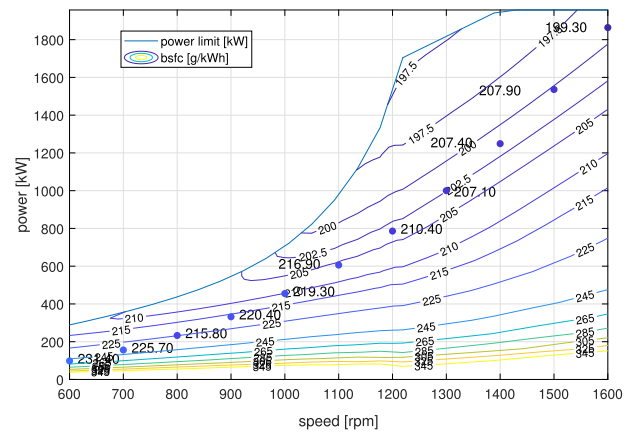


Fig. 9. Fuel consumption map and relative errors.

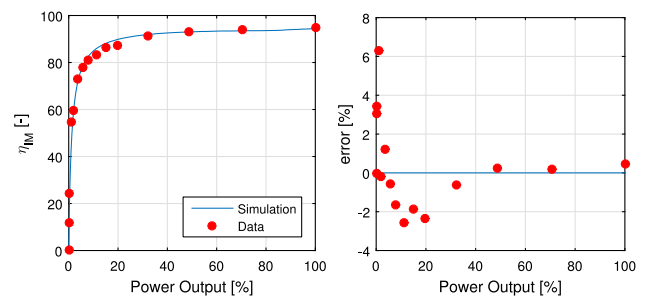


Fig. 10. Combined efficiency of induction machine & frequency converter, and relative errors.

c). The comparison between actual measurements and the estimated fuel consumption, shown in Fig. 9 demonstrates that the accuracy of the model is within +/- 5% down to a load of 5%. Further accuracy improvements could be made by including the effects of variable injection timing.

2.10.2. Induction machine and frequency converter

The necessary parameters for the induction machines and frequency converters were estimated based on supplier data: part-load efficiency, no-load and locked-rotor test results. Fig. 10 illustrates the combined efficiency of the induction machine and frequency converter, which is within +/- 3% of supplier data down to 3% load.

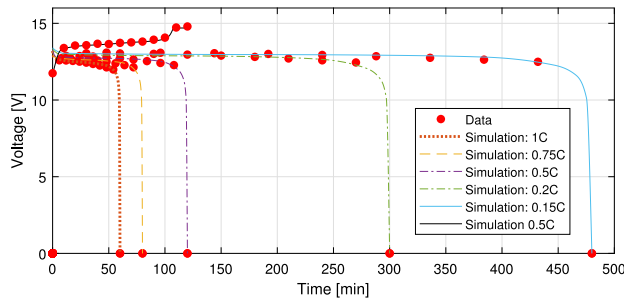


Fig. 11. Battery model: simulation results and supplier data.

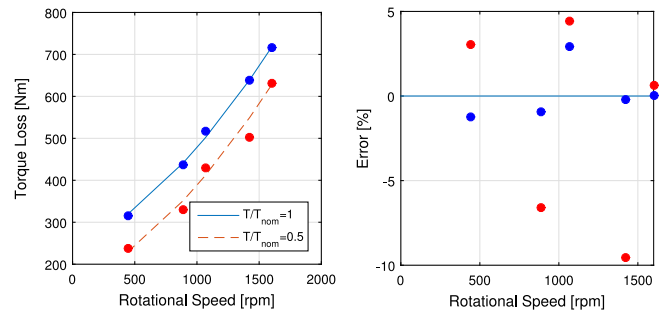


Fig. 14. Simulated and actual torque losses of the gearbox.

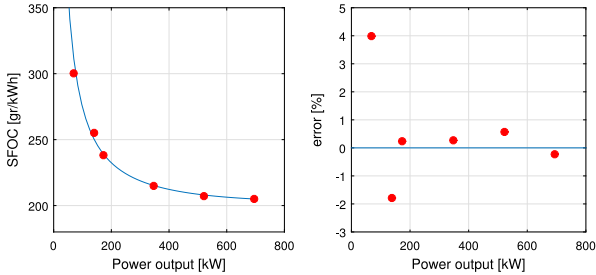


Fig. 12. Simulated Diesel-generator fuel consumption and manufacturer's data.

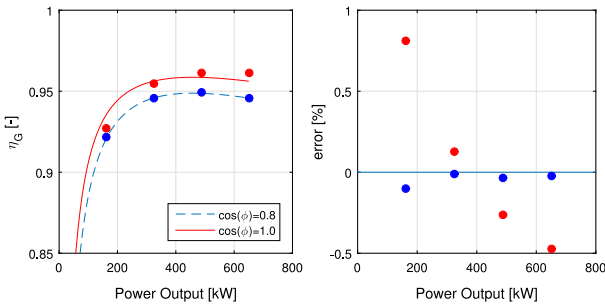


Fig. 13. Synchronous generator efficiency and manufacturer's data.

2.10.3. Battery

We derived the battery values for $\vec{v} = (v_1, \dots, v_6) \in \mathbb{R}^6$ and $\mathbf{A} = (\alpha_{i,j}) \in \mathbb{R}^{3 \times 2}$, $\mathbf{B} = (\beta_{i,j}) \in \mathbb{R}^{2 \times 2}$ from a least-squares errors minimisation problem using typical supplier data of charge/discharge characteristics at different C-rates. A comparison between simulation results and the supplier data is shown in Fig. 11.

2.10.4. Diesel-generator set

The model parameters for the diesel generator were estimated using supplier's data. Figs. 12–13 give a comparison between estimated and actual values. In terms of fuel consumption the error has a maximum of 4% at 10% load, whereas the error of the efficiency of the synchronous generator is lower than 0.8% throughout, and almost negligible for a power factor of 0.8.

2.10.5. Propeller

The model uses the results of the propeller open water tests for the Wageningen K_a5-75 propeller series with nozzle 19A (Kuiper, 1992), which is a well accepted method to model propeller thrust and torque within the assumptions of a homogeneous advance speed, perpendicular flow into the propeller and quasi static performance. Validation of the behaviour of the propeller model in the ship as a whole is covered in Geertsma et al. (2017b).

2.10.6. Gearbox and shaftline

The model parameters for the gearbox and shaft-line are estimated using on-board measurements. The differences can be seen in Fig. 14, with a maximum error of 10%.

3. Energy management strategies

The Energy Management Strategies proposed in this paper determine the load split between the main engines (MEs) and the induction machines (IMs) for hybrid propulsion and between the diesel generator (DG) and battery packs (BAT) for hybrid power generation. The speed setpoints for propulsion are determined by the speed setpoint from the operator for the MEs $n_{me, set}$, when running, and for the IMs $n_{im, set}$, when the MEs are off. The power split between the MEs and IMs, when both are running in parallel, is established with the torque setpoint for the IMs $M_{im, set}$. The speed setpoint for the DG, when running, and the BAT when the DG is off, is fixed with the 60 Hz electrical network frequency, at 30 Hz, due to the 2 pole pairs p_p of the synchronous generator. The power split between the DG and BAT, when both are operating in parallel, is established with the current setpoint for the frequency converter of the BAT $I_{bat, set}$. Therefore, the Energy Management Strategies have to determine the torque setting of the Induction Machines $M_{im, set}$, the current setting of the Battery $I_{bat, set}$ and the binary settings for switching the MEs, IMs, DG and BAT on or off ($b_{dg}, b_{im}, b_{me} \in \mathbb{Z}_2$), as illustrated in Fig. 4. The aim of the strategies is to minimise fuel consumption over the operating profile between two consecutive recharging opportunities, using real-time optimisation.

ECMS was initially introduced by Paganelli (1999) and is based on the notion that battery can be seen as an auxiliary, reversible fuel tank. Therefore, by assigning a cost to electrical energy, it can be associated with a certain quantity of fuel. This cost is known as equivalence factor or co-state $s(t)$. It is the key control parameter of ECMS, and largely dictates its performance. The equivalence factor represents the chain of efficiencies through which fuel is transformed into electrical power and vice versa. As such, it changes for each operating condition of the power-train. In the original formulation of ECMS, the equivalence factor is a set of constants which can be interpreted as the average overall efficiency of the electric path for each operating mode (charge or discharge) for a given mission (Guzzella et al., 2007; Jager, Keulen, & Kessels, 2013; Onori, Serrao, & Rizzoni, 2016; Sciarretta et al., 2004; Sciarretta & Guzzella, 2007). Since the entire mission is usually not known at the outset, any uncertainties about future operating conditions are transferred to uncertainty about the optimal value of the equivalence factor. State-to-costate feedback is applied in most studies, most commonly in the form of a PI-controller (Ambuhl & Guzzella, 2009; Ambuhl et al., 2007; Chasse, Pognant-Gros, & Sciarretta, 2009; Kessels, Koot, Van Den Bosch, & Kok, 2008). However, more advanced feedback laws have also been reported in literature for land-based vehicles, which update the equivalence factor's values based on estimations about future operating conditions or driving pattern recognition (Musardo, Rizzoni, Guezenne, & Staccia, 2005; Onori & Serrao, 2011; Serrao et

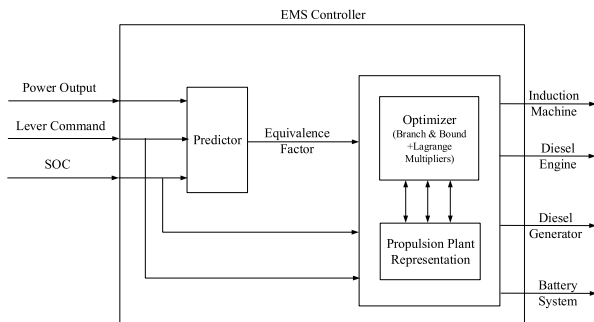


Fig. 15. Schematic overview of the EMS controller.

al., 2013; Sivertsson & Eriksson, 2015). Multiple co-states have also been reported, to include engine and catalyst temperatures in the control objective (Maamria, Sciarretta, Chaplain, & Petit, 2017).

In this work, two different approaches are investigated: The simplest scenario of an ECMS with constant equivalence factor, which has been discussed in Delprat, Guerra, and Rimaux (2002), Guzzella and Onder (2009) and Sciarretta and Guzzella (2007) and applied in Won, Langari, and Ehsani (2005) with a unity value, and a more sophisticated approach of an adaptive equivalence factor based on operator load estimation, as discussed in Vu (2015) and Vu et al. (2014). The schematic representation of the adaptive strategy is illustrated in Fig. 15. It consists of an optimiser that minimises the control objective subject to the applicable constraints, and a ‘predictor’ to estimate the equivalence factor according to (Vu, 2015; Vu et al., 2014). The constant equivalence factor approach is represented by the optimiser only, which has a fixed equivalence factor as its input.

In order to evaluate the performance of the proposed ECMS, we use the dynamic simulation model in Section 2 to compare ECMS against the performance of a rule-based controller and against the global optimum, established with Dynamic Programming (DP), assuming apriori knowledge of the operating profile. The rule based controller is described in Section 3.6 and the DP algorithm in Section 3.7.

3.1. Model reduction

Ideally, the dynamic model presented in Section 2 would be used in the proposed strategies, however, real-time decisions would not be feasible. Furthermore, quasi-static models suffice to a large extent for fuel economy estimation, as dynamic transient behaviour hardly influences total fuel consumption over an entire operating profile (Guzzella et al., 2007; Karlsen, 2012; Sciarretta et al., 2014; Serrao, Hubert, & Rizzoni, 2007). For this reason, energy efficiency of each component will be estimated using efficiency maps, which are highly accurate for fuel consumption estimation, similar to the approach in many automotive ECMS (Sciarretta et al., 2014). These efficiency maps have subsequently been approximated by uni- and bivariate second-degree polynomials, due to their fine balance between accuracy and simplicity. Moreover, the convex character of these polynomials allows computationally fast online optimisation. The accuracy of this approach is discussed at the end of the section.

3.1.1. Main engine

The fuel consumption map of the main engines can be approximated with a quadratic relationship with respect to power output P_{me}^* in W, and engine rotational speed n_{me}^* , as proposed in Shi et al. (2010), as follows:

$$\dot{m}_{f,me}^*(t) = \begin{cases} \alpha_0 + \alpha_1 n_{me}^*(t) + \alpha_2 P_{me}^*(t) + \alpha_3 n_{me}^{*2}(t) + \\ + \alpha_4 P_{me}^{*2}(t) + \alpha_5 n_{me}^*(t)P_{me}^*(t), & 0 < P_{me}^* \leq 1 \\ 0, & P_{me}^* = 0 \end{cases} \quad (65)$$

with $\alpha_i \in (0, 1)$, $i = 1, \dots, 5$ fitted parameters. The accuracy of this approach is illustrated in Fig. 17.

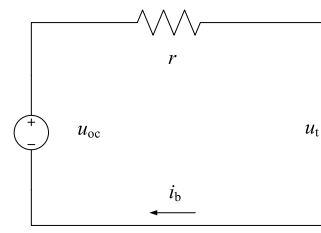


Fig. 16. Battery equivalent circuit representation in the controller.

3.1.2. Induction machine & frequency converter

The combined power losses are estimated based on torque output M_{im}^* in Nm, and shaft rotational speed n_{im}^* . Due to asymmetries in the efficiency between motoring and generating conditions, two different sets of coefficients are necessary, as follows:

$$P_{im+fc,loss}^*(t) = \begin{cases} \epsilon_{i1}n_{im}^*(t) + \epsilon_{i2}M_{im}^*(t) + \epsilon_{i3}n_{im}^{*2}(t) + \\ + \epsilon_{i4}M_{im}^{*2}(t) + \epsilon_{i5}n_{im}^*(t), \\ M_{im}^*(t), & 0 < M_{im}^* \leq 1 \\ 0, & M_{im}^* = 0 \end{cases} \quad (66)$$

$$P_{fc}(t) = P_{im}(t) + P_{im+fc,loss}(t) \quad (67)$$

with $\epsilon_{ij} \in (0, 1)$, $i = 1, 2$, $j = 0, \dots, 5$ fitted parameters. The accuracy of this approach is illustrated in Fig. 17.

3.1.3. Diesel-generator

Fuel consumption of the diesel driving the generator represents a quadratic relationship with respect to rotational speed and power output. Because the diesel generator (DG) operates at constant speed, a one-dimensional polynomial can be used to approximate fuel consumption of the DG, as follows:

$$\dot{m}_{f,dg}^*(t) = \begin{cases} \beta_0 + \beta_1 P_{dg}^*(t) + \beta_2 P_{dg}^{*2}(t), & 0 < P_{dg}^* \leq 1 \\ 0, & P_{dg}^* = 0, \end{cases} \quad (68)$$

with $\beta_i \in (0, 1)$, $i = 0, 1, 2$ fitted parameters. The accuracy of this approach is illustrated in Fig. 17.

3.1.4. Battery

The Ragone efficiency is needed for the objective function (Sciarretta & Guzzella, 2007), and SOC and terminal voltage for the constraints. The open cell voltage is given by Eq. (41), and the efficiency depends on power output, as follows:

$$\eta_{bat}(t) = \delta_0 + \delta_1 P_{bat}(t) + \delta_2 P_{bat}^2(t), \quad (69)$$

with δ_i , $i = 0, 1, 2$ fitted parameters. In order to estimate state of charge and bounded battery power, the equivalent circuit of Fig. 16 is used.

When a current flows in the circuit, the following relations hold:

$$\left. \begin{aligned} i_{bat}(t) &= \frac{P_{bat}(t)}{u_t(t)} \\ u_{oc}(S_{OC}(t)) - ri_{bat}(t) &= u_t(t) \\ u_t^2(t) - u_{oc}(S_{OC}(t))u_t(t) + P_{bat}(t)r_{ec} &= 0. \end{aligned} \right\} \Rightarrow \quad (70)$$

Solving Eq. (70) for power yields:

$$P_{bat}(t) = \frac{-u_t^2(t) + u_t(t)u_{oc}(S_{OC}(t))}{r_{ec}}. \quad (71)$$

Now, upper and lower limits for battery power can be determined:

$$P_{bat,max}(t) = \frac{u_{oc}(S_{OC}(t))u_{t,min} - u_{t,min}^2}{r_{ec}} \quad (72)$$

$$P_{bat,min}(t) = -\frac{u_{t,max}^2 - u_{oc}(S_{OC}(t))u_{t,max}}{r_{ec}}, \quad (73)$$

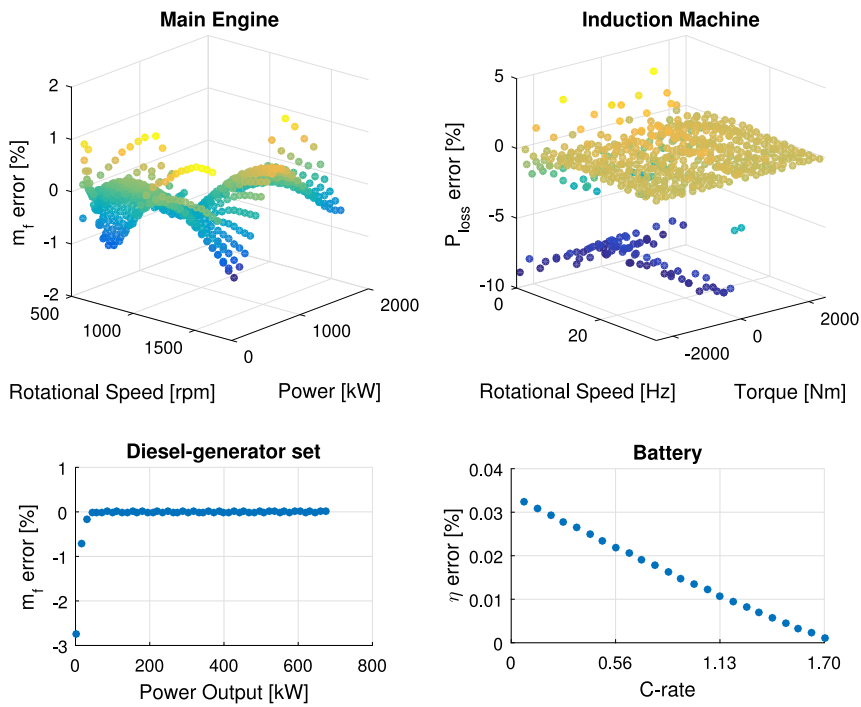


Fig. 17. Fitting errors of Eqs. (65), (66), (68) and (69).

where $u_{t,\min}$ and $u_{t,\max}$ are the manufacturer's terminal voltage limits.

While the Energy Management Strategies (EMS) use state of charge S_{oc} as an exogenous input, the EMS strategy needs to ensure that the SOC limitations are not violated while establishing the next iteration of settings. Therefore, the state of charge after one iteration is established with the more simple first order equivalent circuit (EC) model, illustrated in Fig. 16, as opposed to the second order EC model in the dynamic model. This simple EC model is sufficiently accurate for this purpose as it only influences state of charge S_{oc} over one iteration of the Energy Management Strategy as opposed to the accumulative drift for the dynamic model. Therefore, within the Energy Management Strategies, state of charge S_{oc} is estimated as follows (Koot et al., 2005):

$$\begin{aligned} S_{oc}(t) &= \frac{Q_{bat}(t_0) - \sum_{t=0}^t \left(\frac{P_{bat}(t)}{u_{oc}(S_{oc}(t))} \Delta t \right)}{Q_{bat,nom}} \\ &= S_{oc}(t - \Delta t) - \frac{P_{bat}(t) \Delta t}{u_{oc}(S_{oc}(t)) Q_{bat,nom}}. \end{aligned} \quad (74)$$

Finally, for the battery's rectifier, a constant efficiency η_{rec} is assumed, equal to 97.5%.

Fig. 17 illustrates the accuracy of the relations used, relative to the benchmark simulation model, which is used to evaluate performance against. The induction machine reduced model, in the top-right graph, is within +/- 1% accurate in its normal operating region. While the model is not very accurate around the zero torque and zero speed region, this does not pose a problem for the optimisation process as the IM is indeed inefficient around these regions, and the EMS should avoid operating it. By overestimating the losses around these regions, we actually bias the controller to avoid these regions altogether. For all other components, main engines, diesel generator and battery packs, the accuracy of the model is within 1% and therefore sufficiently accurate to be used for the ECMS approach.

3.2. Optimisation problem formulation

The control objective of ECMS is to establish the control variables BAT current i_{bat} when the DG is running, and IM torque M_{im} when the

MEs are running, in order to minimise the instantaneous equivalent fuel consumption of the vessel $m_{f,eqv}$, subject to propeller speed n_p , power demand for propulsion, P_{pd} , demanded auxiliary power P_{aux} , BAT state of charge S_{oc} , and three binary variables $(b_{dg}, b_{im}, b_{me}) \in \mathbb{Z}_2$ for the ON/OFF state of each component. BAT current i_{bat} and IM torque M_{im} are established from the ECMS control variables BAT power P_{bat} and IM power P_{im} , as follows:

$$i_{bat}(t) = \frac{P_{bat}}{\sqrt{3}u_{line}(t)\cos(f_p)} \quad (75)$$

$$M_{im}(t) = \frac{P_{im}(t)}{2\pi i_{gb} n_p(t)}. \quad (76)$$

While propulsion power demand P_{pd} and shaft speed are a result of the model dynamics against the specified shaft speed setting n_{set} , towing force X_{tow} , resistance curve $R(v_s)$ and auxiliary load P_{aux} in the benchmark dynamic model, the reduced order model requires exogenous inputs propeller speed n_p , power demand for propulsion, P_{pd} , demanded auxiliary power P_{aux} and BAT state of charge S_{oc} . Propulsion power demand subsequently dictates ME power P_{me} when the IMs and MEs are running in parallel, or IM power P_{im} when the MEs are off, through the following equality:

$$P_{me}(t) = P_{pd}(t) - P_{im}(t). \quad (77)$$

Similarly, auxiliary power P_{aux} dictates DG power P_{dg} when the DG and battery packs are operating in parallel, or battery power P_{bat} when the DG is off, with the following equality:

$$P_{dg}(t) = P_{aux}(t) + 2(P_{im}(t) + b_{im}(t)P_{im+fc,loss}(t)) - P_{bat}(t). \quad (78)$$

The equivalent fuel consumption aims to reduce the global optimisation problem of minimising fuel consumption over the operating profile to an instantaneous optimisation of equivalent fuel consumption. To achieve this a cost is assigned to the use of the battery in discharge mode, equivalent to the expected amount of fuel consumption required to recharge the battery and a negative cost is assigned to charging the battery, equivalent to the expect amount of fuel to be saved when the battery is used to provide power (Paganelli, Delprat, Guerra, Rimaux, & Santin, 2002). When the strategy aims to discharge to battery to its

minimum SOC, this can be achieved by reducing the cost assigned to the use of the battery. Therefore, the equivalent fuel consumption is the sum of MEs and DG fuel consumption $\dot{m}_{f,me}$, $\dot{m}_{f,dg}$, and the artificial fuel consumption of the battery packs $\dot{m}_{f,bat}$, and can be defined as follows:

$$\dot{m}_{f,eqv}(t) = \sum_i \dot{m}_{f,me_i}(t) + \dot{m}_{f,dg} + \dot{m}_{f,bat}(t). \quad (79)$$

The artificial fuel consumption of the battery packs is proportional to the equivalence factor s , which differs whether the battery packs are being charged or discharged. In the original formulation of ECMS (Paganelli, 1999), the equivalence factor is a vector of values, one for charge and one for discharge $s(t) = [s_{chg}(t), s_{dis}(t)]$, as follows:

$$s_{dis} = s(t)\eta_{bat}(P_{bat}(t)) \\ s_{chg} = \frac{s(t)}{\eta_{bat}(t)} = s(t)\eta_{bat}^{-1}(P_{bat}(t)). \quad (80)$$

However, since the original ECMS formulation, Kirk (2012) showed that there is no need for multiple factors, since the efficiencies along the electrical path, apart from the battery packs, can be implicitly taken into account using one parameter, as follows:

$$\dot{m}_{f,bat}(t) = c_{sfo,eqv}(t)P_{bat}(t) = \\ = \frac{s(t)}{\eta_{bat}(P_{bat}(t))^{sgn(P_{bat}(t))}} \frac{P_{bat}(t)}{Q_{lhv}}. \quad (81)$$

Utilising the model reduction defined in (65), (66), (68) and (69) and Equalities (77) and (78), the equivalent fuel consumption of Eq. (79) can be summarised as a function of the five control variables $u_c \triangleq [P_{bat}, P_{im}, b_{dg}, b_{im}, b_{me}]$ and exogenous inputs $w_e \triangleq [n_p, P_{pd}, P_{aux}, S_{oc}]$, as follows:

$$\dot{m}_{f,eqv}(t) = 2b_{me}(t)m_{f,me}(n_p(t), P_{pd}(t), P_{im}(t)) \\ + b_{dg}(t)m_{f,dg}(P_{aux}(t), P_{im}(t), b_{im}(t), n_p(t)) \\ + \frac{s(t)}{\eta_{bat}(P_{bat}(t))P_{bat}(t)^{sgn(P_{bat}(t))}} \frac{P_{bat}(t)}{Q_{lhv}}, \quad (82)$$

where $s(t)$ is constant for ECMS and is established with the adaptive regime described in Section 3.5 for AECMS. The resulting optimisation problem definition is:

$$u_c^0(t) = \arg \min_{u_c} \dot{m}_{f,eqv}(u_c, w_e(t), s(t)). \quad (83)$$

The inequality constraints of the optimisation problem include: the predefined SOC limitations to preserve battery lifetime using (74), as follows:

$$SOC_{min} \leq SOC(t) \leq SOC_{max} \Rightarrow \\ SOC_{min} \leq SOC(t - \Delta t) - \frac{P_{bat}(t) \Delta t}{u_{oc}(SOC(t))Q_{bat,nom}} \leq SOC_{max}; \quad (84)$$

the operating envelope of the MEs from (77), as follows:

$$0 \leq P_{p,dem}(t) - b_{im}(t)P_{im}(t) \leq P_{e,max}(n_e(t))b_e(t); \quad (85)$$

the operating envelope of the DG from (78), as follows:

$$0 \leq P_{aux}(t) + 2b_{im}(t)(P_{im}(t) + P_{im+fc,loss}(t)) - P_{bat}(t) + \\ \leq P_{g,nom}b_{dg}(t); \quad (86)$$

power limitations of the BAT from (72) and (73), as follows:

$$-\frac{u_{t,max}^2 - u_{oc}(SOC(t))u_{t,max}}{r} \leq \frac{P_{bat}(t)}{\eta_{rec}^{sgn(P_{bat}(t))}} \leq \\ \leq \frac{u_{oc}(SOC(t))u_{t,min} - u_{t,min}^2}{r}; \quad (87)$$

the operating envelope of the induction machines, as follows:

$$b_{im}(t)P_{im,min} \leq P_{im}(t) \leq P_{im,max}b_{im}(t); \quad (88)$$

and, finally, one extra constraint to force the energy management strategy to operate on the main engines when the vessel is towing:

$$b_{me}(t) = \begin{cases} 1, & \text{if } X_{tow}(t) > 0 \\ 0, & \text{if } X_{tow}(t) = 0. \end{cases} \quad (89)$$

3.3. Solution method

The resulting optimisation problem can be classified as mixed integer non-linear program. Mixed integer non-linear programs are NP-Hard, so their solution time increases exponentially with the number of dimensions of the problem (Hillier, 2012). Vu et al. (2014) use heuristic search methods (genetic algorithms) to solve the optimisation problem. However, heuristic methods usually produce near-optimum solutions, whereas deterministic methods guarantee optimality of the solution (Hillier, 2012). Key factors in solving MINLPs fast enough are (1) the number of integer variables and (2) whether the problem has any special characteristics that can be exploited. In this case, three discrete variables exist, therefore a Branch & Bound (B&B) method is applicable: It will generate only an $2^3 = 8$ node binary search tree, the sub-problems of which are convex, as Appendix A shows. Combining B&B with the method of Lagrange Multipliers to solve the arising convex sub-problems will result in limited computational time and guaranteed optimality of the solution for the defined problem formulation.

3.4. Constant equivalence factor

In the first energy management strategy, in this work referred to as ECMS, a constant equivalence factor value has been adopted. The idea of a constant equivalence factor has been discussed in several studies in the past (Delprat et al., 2002; Guzzella & Onder, 2009; Sciarretta & Guzzella, 2007), mostly considering how close the resulting solution is to the global optimum. A constant equivalence factor only provides a solution close to the global optimum, when the battery usage is limited to a relatively narrow SOC range, as voltage and resistance do not vary much (Kim, Cha, & Peng, 2011). In Appendix B we investigate the effect of battery's SOC, power input and output to the variation of the equivalence factor. Based on that analysis we have concluded that a constant equivalence factor provides a solution near the global optimum, regardless of the state of the battery packs.

Considering the battery as an auxiliary fuel tank, the value of the equivalence factor is chosen to reflect the nominal fuel consumption of the main engines, corrected for the nominal efficiency of the components between the battery packs and the shaft:

$$s = c_{sfo,e} \eta_{rec} \eta_{im+fc} Q_{lhv} = 2.165. \quad (90)$$

The key concept is that the use of the batteries will prevent low engine loading. Dedes (2013) and Yuan et al. (2016) indicate that, when the load demand falls within the inefficient, low-loading region of the engine, its specific fuel consumption will be higher than the battery pack's. As a consequence, the controller will opt to either (1) switch off all of the engines and operate on the battery packs, or (2) increase engine loading to a more efficient operating point, using the excess power to recharge. The ECMS will chose between these options based on the value of the equivalence factor s , relative to the fuel consumption in the operating point with the increased engine loading, and is limited by the battery power and state of charge constraints. If the low loading operating point would be maintained for a long period in time, this could lead to a start-stop strategy, but this does not occur in the typical operating profile as demonstrated in Section 4 and Fig. 23.

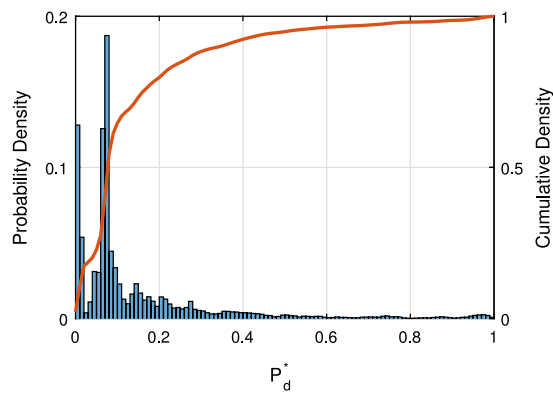


Fig. 18. Measured power demand distribution of tugboats operating in the port of Rotterdam.

3.5. Adaptation based on operating load estimation

In the second strategy, the equivalence factor is estimated on the basis of historical data: using tugboat measurements of operations in the port of Rotterdam, the probability distribution of normalised propulsion power demand $P_{p,dem}^*$ was compiled, shown in Fig. 18, and combined with the propulsive load prediction scheme of Vu (2015) and Vu et al. (2014). This prediction scheme estimates upcoming load changes based on a stochastic approach over a future prediction horizon of 10 min, and is referred to as A-ECMS. The equivalence factor value is set equal to the inverse chain efficiency of the electrical path (battery–rectifier–frequency converter– induction motor) based on the predicted load:

$$s(t) = \prod_{i=1}^4 \frac{1}{\eta_i (1 - \hat{P}_{p,dem}^*(t))}. \quad (91)$$

Furthermore, a penalty function has been used to guarantee that the SOC does not exceed the admissible limits, $S_{OC_{min}} \leq S_{OC}(t) \leq S_{OC_{max}}$, as follows:

$$\mu = \begin{cases} 1 - \left(\frac{S_{OC_a} - S_{OC}(t)}{\sigma} \right)^a & \text{for } S_{OC}(t) \leq S_{OC_a} \\ 1 & \text{for } S_{OC_a} \leq S_{OC}(t) \leq S_{OC_b} \\ 1 - \left(\frac{S_{OC}(t) - S_{OC_b}}{\sigma} \right)^a & \text{for } S_{OC}(t) \geq S_{OC_b}, \end{cases} \quad (92)$$

with:

$$\sigma = \frac{S_{OC_{max}} - S_{OC_{min}}}{2}$$

$$S_{OC_{min}} \leq S_{OC_a} \leq S_{OC_b} \leq S_{OC_{max}}.$$

Its effect can be seen in Fig. 19, penalising for the SOC being close to the lower or upper bound $S_{OC_{min}}, S_{OC_{max}}$.

3.6. Rule-based control

The rule-based controller in this study is used to compare the performance of the Energy Management Strategies with a commercially available rule-based controller, that has been applied to the actual case study tug. This controller switches between three operating modes for propulsion, as described in (de Groot & van Koperen, 2014): standby, free sailing mode. These three mode are defined, as follows:

- In standby mode, when the speed setting of the propulsion plant n_{set} ranges from 0 to 8.33 Hz, or 0 rpm to 500 rpm, the main engines (MEs) and diesel generator (DG) are switched off and the ship is propelled with the induction machines (IMs). Power to the IMs is provided by the battery packs (BAT) until they reach their

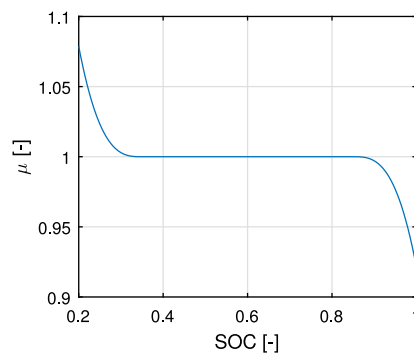


Fig. 19. Effect of multiplicative penalty function $\mu(S_{OC})$ of Eq. (91).

minimum state of charge (SOC) S_{OC} , at 20% SOC. Then the DG is started and will provide electrical power to the IMs and charge the BAT at its maximum rate within the constraints of maximum DG power.

- In free sailing mode, when the speed setting of the propulsion plant n_{set} is higher than 8.33 Hz, or 500 rpm, either the DG or the MEs provides auxiliary and propulsion power. In the speed setting n_{set} range from 8.33 to 15 Hz, or 500 to 900 rpm, the MEs are switched off and the IMs provide propulsion power. The DG is switched on and provides electrical power for propulsion, auxiliaries and battery charging. The battery packs are charged at its maximum rate within the constraints of maximum DG power. In the speed setting n_{set} range from 15 Hz to 30 Hz, or 900 to 1800 rpm, the MEs provides power for propulsion and the IMs. Moreover, the IMs, driven by the MEs, operate as generator and provide electrical power to the auxiliary load and charge the BAT at its maximum rate within the constraints of maximum IMs power.
- In towing mode, the MEs are switched on regardless of the speed setting, in order to ensure full bollard pull is directly available without notice. The MEs provide power for propulsion and the IMs. Moreover, the IMs, driven by the MEs, operate as generator, provide electrical power to the auxiliary load and charge the BAT at its maximum rate within the constraints of maximum IMs power.

3.7. Global optimum for known operating profile

The ECMS and A-ECMS are causal sub-optimal control strategies as they have very limited information on future operating conditions. Thus, their decision quality is limited. The entire mission is usually unknown from the outset, therefore adaptive controllers have to rely on estimations of future operating conditions. Because the operating profiles assessed in this study are known, the causal controllers can be compared with a non-causal optimal controller that has been determined using Dynamic Programming (DP). The generic DP MATLAB function of Elbert, Ebbesen, and Guzzella (2013), Sundstrom, Ambuhl, and Guzzella (2010) and Sundstrom and Guzzella (2009) has been used to provide the global optimum solution.

4. Controller evaluation

4.1. Simulation experiments

With the simulation models described in Section 2, we have analysed the fuel consumption for the case study tug with hybrid propulsion. The MATLAB Simulink R2014b software has been used on a PC with Intel Core i7 processor and 16 GB memory to simulate the hybrid propulsion

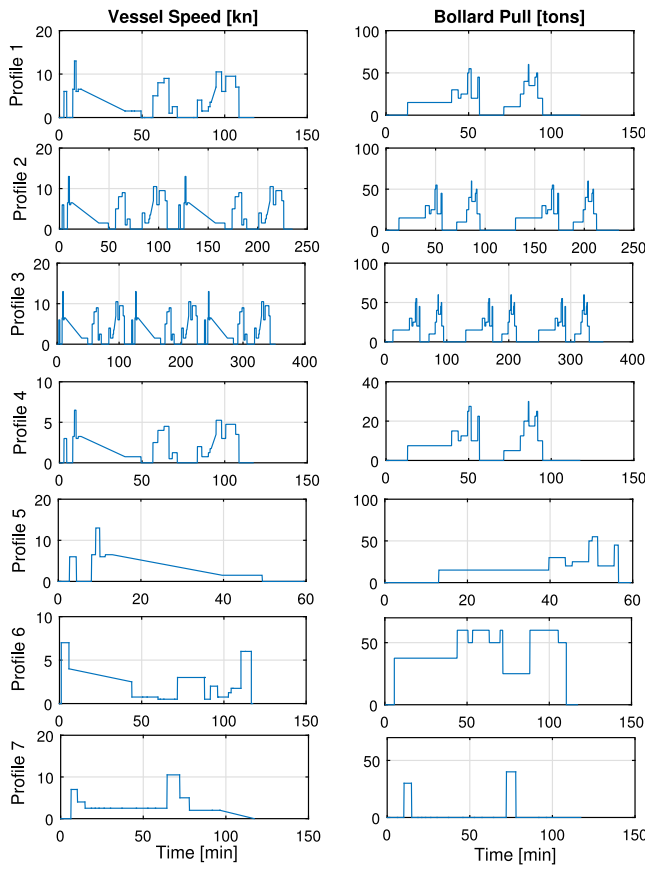


Fig. 20. Simulated operating profiles.

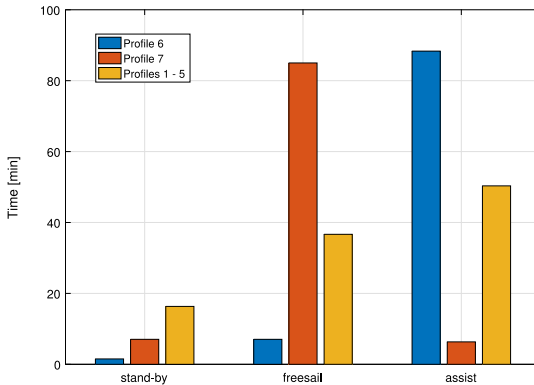


Fig. 21. Standard, idle and busy operating profiles — operating mode distribution.

plant. To objectively assess the performance and robustness of the proposed suboptimal control system, we have compiled 6 variations of a real operating profile shown in Fig. 20. Profile 1 is the standard profile, and is based on measurements of tugboats operating in the port of Rotterdam. Profiles 2 and 3 are two and three times the duration of the standard profile. Profile 4 represents a ‘lighter’ loading variation, in which vessel speed and bollard pull have been reduced in half, and profile 5 represents a shorter mission, of roughly half the duration of the standard profile. Finally, Profile 6 represents an extremely busy profile, consisting of tow jobs with heavy loads, and Profile 7 is an idle profile, in which the vessel is mostly free-sailing at low speeds. The difference between the first five ‘original’ missions (Profiles 1–5), the busy profile

Table 1

Results from simulation experiments with rule-based (RB) control, Equivalent Consumption Minimisation Strategy (ECMS), adaptive ECMS (A-ECMS) and causal control with dynamic programming (DP) for operating profiles defined in Section 4.1.

EMS	Fuel				
	m_f [kg]	Savings [%]	$S_{OC,f}$ [%]	η_{vessel} [%]	
Profile 1	DP	336.1	7.79	20	35.5
	RB	364.5	—	94	36.0
	ECMS	340.1	6.62	31	35.3
	A-ECMS	343.2	5.71	36	35.8
Profile 2	DP	846.8	3.49	20	36.6
	RB	876.9	—	94	36.1
	ECMS	869.6	0.83	33	36.0
	A-ECMS	857.9	2.27	27	36.0
Profile 3	DP	1104.3	2.62	20	36.4
	RB	1134.1	—	94	36.2
	ECMS	1118.6	1.36	35	36.1
	A-ECMS	1122.8	0.99	30	36.0
Profile 4	DP	259.6	10.5	27	35.6
	RB	290.0	—	100	35.1
	ECMS	270.1	6.89	20	34.9
	A-ECMS	264.3	8.96	20	35.0
Profile 5	DP	161.8	17.35	25	35.4
	RB	195.9	—	100	35.8
	ECMS	174.6	10.85	66	35.2
	A-ECMS	177.6	9.32	61	35.1
Profile 6	DP	1039.4	3.51	20	38.9
	RB	1077.3	—	95	38.6
	ECMS	1047.1	2.77	37	38.7
	A-ECMS	1046.3	2.81	33	38.5
Profile 7	DP	224.6	16.07	20	34.8
	RB	267.6	—	99	34.2
	ECMS	239.2	10.51	20	34.3
	A-ECMS	234.8	12.27	20	34.6

ECMS: Constant equivalence factor.

A-ECMS: Adaptive equivalence factor.

(Profile 6) and idle profile (Profile 7) are shown in Fig. 21. The total time spent in stand-by, free-sailing and assisting modes is visualised.

4.2. Results

Table 1 lists the fuel consumption m_f , savings compared to rule-based (RB) controller in %, state of charge at the end of each mission $S_{OC,f}$ and average vessel efficiency η_{vessel} from the simulation experiments and mission profiles described in Section 4.1. These results confirm that DP yields the lowest fuel consumption for all operating profiles, with an average reduction of 8.6% compared to the currently used rule-based controller, which aims to maintain battery charge. The resulting savings are attributed to better utilisation of the battery packs, reflected by a lower SOC at the end of the mission shown in Fig. 23, rather than the increased efficiency of the propulsion plant. In fact, the global optimum, established with DP, only marginally beats the rule-based controller’s decisions in terms of plant efficiency and only for the longer operating profiles. Therefore, if a charge-sustaining solution was desired, the current rule-based controller provides near optimum solutions. This has been verified by imposing the constraint $S_{OC,f,DP} = S_{OC,f,RB}$ to the causal controller and the results in Table 2, which demonstrate the rule-based controller achieves a solution within approximately 1% of the global optimum.

The cumulative saving of the ECMS strategy over all operating profiles is 3.7%, which is 2.1% less than the global optimum. For typical operating profiles, the saving of ECMS is 5% to 10%, but these savings are not robust for long or heavily loaded operating profiles. The AECMS strategy performs slightly better over the cumulative operating profiles at 4% savings, but ECMS performs better over the typical profile, while

Table 2

Results from simulation experiments with rule-based (RB) control and causal control with dynamic programming (DP) when charge sustainment is imposed, for operating profiles defined in Section 4.1.

	EMS	m_f [kg]	m_f [%]	η_{vessel} [%]	$S_{OC,f}$ [%]
Profile 1	DP	361.3		36.2	
	RB	364.5	101.1	36.0	94
Profile 2	DP	872.1		36.3	
	RB	876.9	100.6	36.1	94
Profile 3	DP	1130.0		36.1	
	RB	1134.1	100.4	36.3	94
Profile 4	DP	288.2		35.3	
	RB	290.0	100.6	35.0	100
Profile 5	DP	193.2		36.1	
	RB	195.9	101.4	35.9	100
Profile 6	DP	1065.4		38.8	
	RB	1077.3	101.1	38.6	95
Profile 7	DP	264.6		34.7	
	RB	267.6	101.2	34.2	99

AECMS performs typically better at low loads, for example profile 4 and 7. Furthermore, the difference between the two strategies does not appear consistent and significant, therefore the adaptive algorithm does not perform consistently better. This is most probably caused by the short time window that the adaptive algorithm looks ahead and the uncertainty of the power demand distribution.

The state of charge and equivalence factor trajectories shown in Fig. 23, demonstrate that the equivalence factor should mostly be increased or decreased when the mission length is increased or decreased. Future work should therefore focus on developing an algorithm that adapts equivalence factor based on the state of charge and remaining mission time or uses a predictive approach with a time window similar to mission length. The maximum additional fuel saving that can be achieved with such approaches is approximately 2%.

While the fuel savings that can be achieved with Energy Management Strategies are significant, the differences between the rule-based controller, both ECMS strategies and the global optimum are significantly smaller than in the study investigating the impact of various Energy Management Strategies for the plug-in hybrid vehicle benchmark studied in Sciarretta et al. (2014). For various operating profiles the difference between various rule-based and ECMS strategies in that study is reported to be 25% to 40%. Analysing the results of these studies, we attribute the smaller difference between various Energy Management Strategies for the tug to three main causes:

- The degree of freedom in control for the operating point of the main engines and the diesel generator is smaller for the tug case, because the energy management strategy cannot influence engine speed, while the planetary gearbox of the plug-in hybrid vehicle allows variable operating speed of the engine (Sciarretta et al., 2014). Main engine speed is fixed, because the relationship between engine speed and torque is fixed by the fixed pitch propeller characteristics in combination with the ships resistance curve. A controllable pitch propeller could enable variable engine speed. Diesel generator speed is fixed at constant frequency, because diesel generator speed dictates electrical network frequency. Diesel generator speed could be made variable, if a DC power distribution system was applied as proposed in Zahedi et al. (2014), who reported fuel savings of up to 15% with a DC power supply with energy storage, of which 7% was attributed to the use of energy storage with the energy management algorithm proposed in Zahedi et al. (2014), for a case study Off-shore Support Vessel (OSV). Future studies could therefore investigate the impact of controllable pitch propellers and DC power supply on Energy Management Strategies, although DC

stability would have to be addressed (Flower & Hodge, 2014; Haseltalab & Negenborn, 2017; Herrera, Zhang, & Wang, 2017; Simmonds, 2014; Zahedi & Norum, 2013). The operating points of the main engine during profile 1 and 4, shown in Fig. 22, clearly demonstrate that all operating points of the main engine are close to the quadratic propeller curve (Geertsma et al., 2017a). Causal global optimum control operates the engine at lower power, in order to reach minimum state of charge at the end of the operating profile, as shown in Fig. 23, while the rule-based and ECMS strategies operate the engine at higher power, but do not achieve minimum state of charge. The global optimum strategy actually accepts the penalty of operating the main engines at a less efficient operating point, in the region where the gradient of fuel consumption as a function of torque is minimal, in order to ensure all stored battery energy is used. Moreover, global optimum control does not load the engine at its maximum load, suggesting an engine with reduced rating could be used, further reducing fuel consumption, as the smaller engine would be running at a higher relative load and thus lower fuel consumption. At maximum bollard pull, the induction machines would then run at full power in parallel with the main engines.

- In a significant part of the operating profile, during towing, the main engines are switched on, to ensure full bollard pull is directly available, without first having to start the main engines. In order to investigate the influence of this constraint, we have run the optimisation algorithms without the constraint to run the main engines during towing. The results in Table 3 demonstrate 2% to 3% additional fuel savings could be achieved if the main engines were not forced on during towing operations. While these savings are significant, they would require a proven reliable and very fast starting system for the main engines, that is equally reliable and safe as running with main engines on during towing continuously.
- A significant amount of fuel savings in plug-in hybrid vehicles is achieved by storing energy regenerated during braking in city traffic or downhill driving. The operating profile of ships does not feature a significant amount of braking or any altitude fluctuation, although crane ships and ships with heave compensation can restore energy during crane or heave compensation operations, and these ship types could definitely benefit more from hybrid power supply (Geertsma et al., 2017a; Ovrum & Bergh, 2015).

For the current equivalence factor, the battery packs appear to be well sized for 2 h missions. Proportionally larger sized batteries would lead to a close to optimum performance of ECMS for longer operating profiles with the typical loading profile. Therefore, the proposed ECMS with the proposed propulsion architecture and battery pack size is likely to achieve close to optimum fuel savings for tugs that operate 2 h missions mostly and can be recharged. ECMS without equivalence factor tuning does not appear to be robust against changes in operating profile length or loading, as the fuel savings for the alternative operating profiles are further away from the global optimum. Nevertheless, both ECMS and AECMS perform better than the current rule-based controller for all operating profiles investigated. Moreover, from this analysis we can conclude that optimum sizing of the battery packs should be established with an integrated co-design approach including the energy management strategy as proposed in Hofman and Janssen (2017), Murgovski, Johannesson, Sjoberg, and Egardt (2012), Silvas, Hofman, Murgovski, Etman, and Steinbuch (2017) and Xu, Nueller, Li, Ouyang, and Hu (2015).

The performance of the ECMS and AECMS strategies compared to the global optimum solution can be analysed with the state of charge and equivalence factor trajectories, as shown in Figs. 23 and 24. These figures compare the state of charge and equivalence factor values of the causal controllers, to the optimal state of charge and equivalence

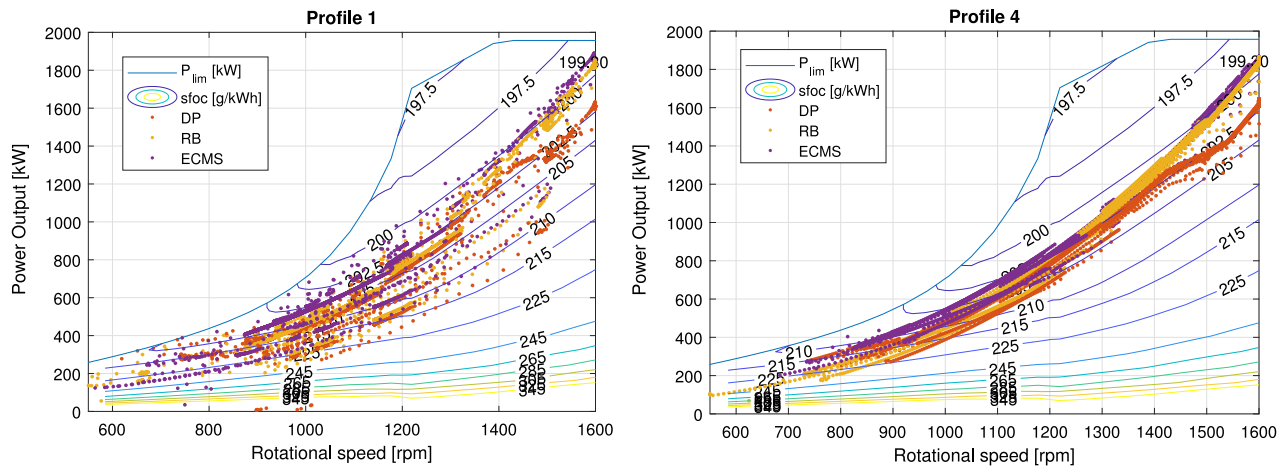


Fig. 22. Operating points of the main engines in the operating envelope for causal global optimum control (DP), rule-based control (RBC) and ECMS during operating profiles 1 and 4.

Table 3

Results from simulation experiments with rule-based (RB) control with towing mode, Equivalent Consumption Minimisation Strategy (ECMS) without towing constraint, and causal control with dynamic programming (DP) with and without towing constraint (wTC and woTC) for operating profiles defined in Section 4.1.

EMS	Fuel		$S_{OC,f}$	η_{vessel}
	m_f [kg]	Savings [%] RB		
Profile 1	DP wTC	336.1	7.79	20
	RB	364.5	–	36.0
	ECMS	332.9	8.67	34
	DP woTC	328.1	9.98	20
Profile 2	DP	846.8	3.49	20
	RB	876.9	–	36.1
	ECMS	855.2	2.47	31
	DP woTC	832.8	5.25	20
Profile 3	DP	1104.3	2.62	20
	RB	1134.1	–	36.2
	ECMS	1107.8	2.32	34
	DP woTC	1092.3	3.68	20
Profile 4	DP	259.6	10.5	27
	RB	290.0	–	100
	ECMS	262.9	9.34	20
	DP woTC	251.6	13.24	23
Profile 5	DP	161.8	17.35	25
	RB	195.9	–	100
	ECMS	171.0	12.71	64
	DP woTC	157.8	19.45	22
Profile 6	DP	1039.4	3.51	20
	RB	1077.3	–	95
	ECMS	1043.5	3.13	36
	DP woTC	1035.4	3.89	20
Profile 7	DP	224.6	16.07	20
	RB	267.6	–	99
	ECMS	232.0	13.30	20
	DP woTC	216.6	18.85	20

ECMS: Constant equivalence factor.

A-ECMS: Adaptive equivalence factor.

factor, derived using the DP solution. The adaptive equivalence factor for typical operating Profile 1 is constantly higher than the optimal, penalising the use of the batteries. On the other hand, better results are achieved with the constant equivalence factor for typical operating Profile 1 due to its closer resemblance to the optimum one. When the equivalence factor of the DP solution varies more, due to long operating profiles or heavy loading, in most cases the AECMS follows the equivalence factor of the global optimum more closely. Finally, an

estimation of an average, near-optimal equivalence factor, can be found by plotting used battery energy $E_B = Q_B \times (S_{OC,0} - S_{OC,f})$ as a function of achieved fuel savings, visualised in Fig. 25. In fact, the derivative of this approximately linear pattern equals 178 g/kWh, corresponding to an equivalence factor value of 2.15, 0.7% lower than our initial estimate.

Fig. 23 also demonstrates the rule-based controller only uses the battery packs occasionally. Moreover, without recharging, the battery packs would not reach its minimum state of charge for any of the investigated operating profiles. Therefore, a quick-win can be achieved by modifying the rule-based controller to not recharge the battery packs, or to only recharge the battery packs, when its SOC reaches a certain value and the main engines are running at high efficiency. Future research could investigate the impact of this modification of the rule-based controller with the methodology proposed in this work.

5. Conclusions and further work

Hybrid propulsion and power generation will play an important role in marine transportation, due to its fuel consumption and CO₂ reduction benefits. In this work, we have applied and benchmarked two ECMS-based controllers to a tugboat with a rule-base controlled hybrid propulsion and power generation plant, and demonstrated that ECMS can contribute significantly to cleaner shipping, particularly if we recharge the batteries from the shore grid in between missions. Simulation results demonstrate that fuel savings and associated CO₂ emission reductions of 5% to 10% can be achieved with the proposed methods for a typical operating profile, within 1%–2% of the global optimum solution. While the near optimum performance of ECMS is not robust against changes in operating profile length or heavy loading, ECMS does perform better than a charge sustaining rule-based controller and the charge sustaining global optimum for all operating profiles investigated. Furthermore, by testing the robustness of the strategies against contrasting profiles we demonstrated that, although better fuel economy than charge sustaining rule-based control is achieved in any case, the strategy can be improved by either including adaption of the equivalence factor based on remaining mission time or using a predictive approach with a prediction horizon as long as the time between recharging opportunities.

Future work should therefore focus on developing an algorithm that adapts the equivalence factor based on the SOC and remaining mission time or uses a predictive approach with a time window similar to mission length. Moreover, the dynamic simulation models proposed in this study can be used to analyse dynamic performance and determine whether engine thermal loading can be reduced and acceleration times improved with hybrid propulsion and power generation. Finally, the controller design should be included in optimisation studies of the

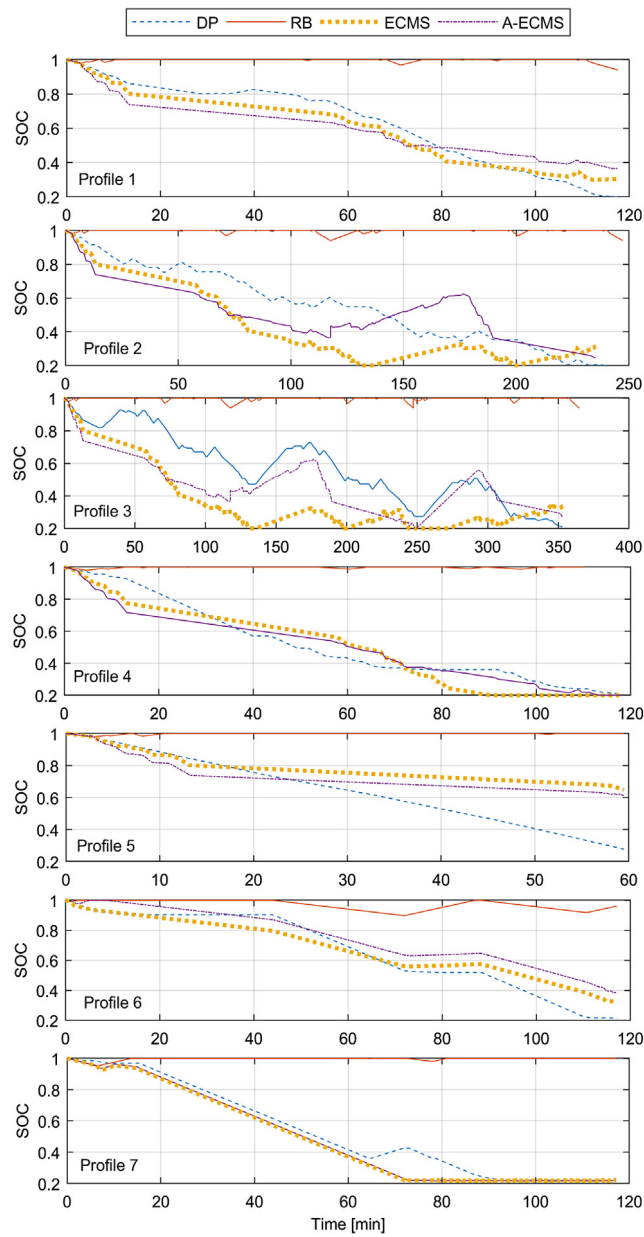


Fig. 23. State Of Charge (SOC) trajectories for all operating profiles.

hybrid propulsion and power generation plant, in order to determine optimal sizing for the main engines, induction machines, diesel generators and batteries.

Acknowledgements

This project is partially supported by project ‘ShipDrive: A Novel Methodology for Integrated Modelling, Control, and Optimization of Hybrid Ship Systems’ (project 13276) of the Netherlands Organisation for Scientific Research (NWO), domain Applied and Engineering Sciences (TTW) and by the Royal Netherlands Navy.

Special thanks goes to Damen Shipyards group for supplying all relevant information about the hybrid tug, along with their data logs regarding usual operating conditions in the port of Rotterdam, onboard measurements used for calibration of the gearbox model, sea trial data to calibrate the resistance curve and the commercially operated rule-based controller.

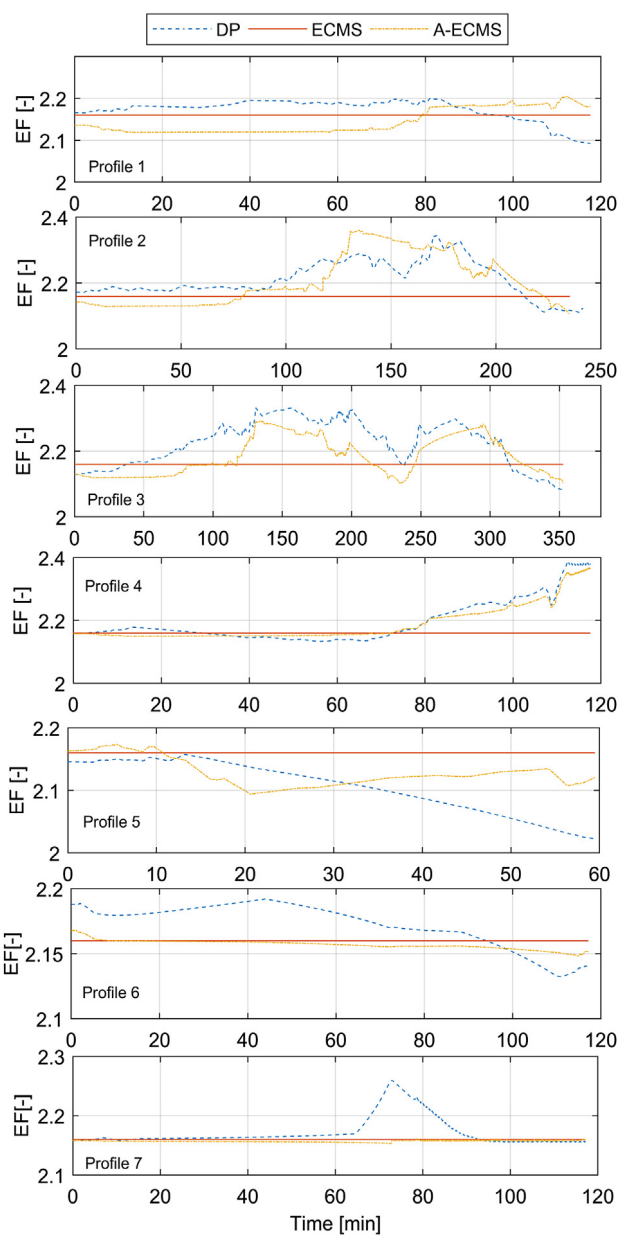


Fig. 24. Equivalence Factor trajectories for all operating profiles.

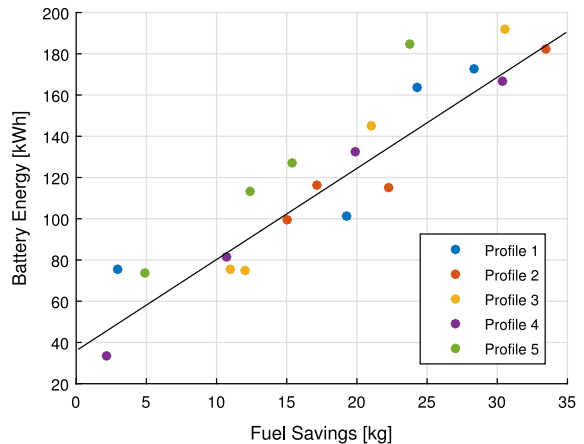


Fig. 25. Battery energy as a function of achieved fuel savings.

Appendix A. Convexity of the optimisation problem

Below, we give a mathematical proof that the continuous relaxation of the optimisation problem is Convex.

A.1. Definitions & theorems

Below we have listed the necessary definitions and theorems for our proof:

Definition 1 (Convexity). A function f is convex if $\text{dom } f$ is a convex set and if for all $x, y \in \text{dom } f$, and θ with $0 \leq \theta \leq 1$ we have:

$$f(\theta x + (1 - \theta)y) \leq \theta f(x) + (1 - \theta)f(y)$$

Definition 2 (Positive semi-definite matrix). A symmetric $n \times n$ real matrix M is said to be positive semi-definite if the scalar $z^T M z$ is non-negative for every non-zero column vector z of n real values.

Theorem 1 (First-order conditions). Supposing f is differentiable (i.e., its gradient ∇f exists at each point in $\text{dom } f$, which is open). Then f is convex if and only if $\text{dom } f$ is convex and:

$$f(y) \geq f(x) + \nabla f(x)^T(y - x)$$

for all $x, y \in \text{dom } f$

Theorem 2 (Second-order conditions). Supposing f is twice differentiable, that is, its Hessian or second derivative $\nabla^2 f$ exists at each point in $\text{dom } f$. Then f is convex if and only if $\text{dom } f$ is convex and its Hessian is positive semidefinite.

Theorem 3 (Convexity preservation: Weighted sums). If f_1, f_2, \dots, f_n are convex functions and $w_1, w_2, \dots, w_n \geq 0$, then the weighted sum:

$$f = w_1 f_1 + \dots + w_n f_n$$

is convex.

Theorem 4 (Convexity preservation: Composition). Given the functions g in $\text{dom } g$ and h in $\text{dom } h$, function f defined by:

$$f(x) = (h \circ g)(x) \text{ with } \text{dom } f = \{x \in \text{dom } g \mid g(x) \in \text{dom } h\}$$

is convex when one of the following statements is valid:

- h is convex, \bar{h} is non-decreasing, and g is convex.
- h is convex, \bar{h} is non-increasing, and g is concave.

where \bar{h} denotes the extended-value extension of function h , which assigns the value $+\infty$ ($-\infty$) to points not in $\text{dom } h$ for h convex (concave).

A.2. Convexity of the problem

To assist readability, we use different notation to address each function and the decision variables, according to Table A.4. We will consider only the most general case for which all the components are operating. However, it will become evident that convexity holds for any combination of operating components.

The control objective can be written as follows:

$$f(x, y) = 2f_1(x) + f_2(x, y) + f_3(y)$$

According to Theorem 3, we need to show that each of f_i , $i = 1, 2, 3$ are convex. One complication is that Theorem 3 refers to functions defined on the same domain, which is not the case for f_1 and f_3 . However, Theorem 3 applies in this case as well. If $f(x)|x \in \mathbb{F}$ and $g(y)|y \in \mathbb{G}$ are convex $h(x, y) = f(x) + g(y)$ is also convex in the domain $\{x \in \mathbb{F} | y \in \mathbb{G}\}$ by definition:

Table A.4
Notation used in this section.

Reference	New symbol
M_{im}	x
P_{bat}	y
$\dot{m}_{\text{f},\text{eqv}}(M_{\text{im}})$	$f(x)$
$\dot{m}_{\text{f},e}(M_{\text{im}})$	$f_1(x)$
$\dot{m}_{\text{f},\text{dg}}(M_{\text{im}}, P_{\text{bat}})$	$f_2(x, y)$
$\dot{m}_{\text{bat}}(P_{\text{bat}})$	$f_3(y)$
$P_{\text{im},\text{loss}}(M_{\text{im}})$	$q(x)$

Let $z_1 = (x_1, y_1)$ and $z_2 = (x_2, y_2)$, then:

$$\begin{aligned} h(\theta z_1 + (1 - \theta)z_2) &= h(\theta x_1 + (1 - \theta)x_2, \theta y_1 + (1 - \theta)y_2) = \\ &= f(\theta x_1 + (1 - \theta)x_2) + g(\theta y_1 + (1 - \theta)y_2) \leq \\ &\theta f(x_1) + (1 - \theta)f(x_2) + \theta g(y_1) + (1 - \theta)g(y_2) = \\ &= \theta h(z_1) + (1 - \theta)z_2 \end{aligned}$$

A.3. Main diesel engine fuel consumption

Function $f_1(x)$ can be written as a scalar composition of two functions, g and h , and convexity can be proven using Theorem 4. $g(x)$ refers to the normalised main engine power output as a function of induction machine torque output, and $h(g(x))$ indicates main engine's fuel consumption, as a function of power output and shaft speed (see Eq. (65)):

$$f_1(x) = (h \circ g)(x),$$

with $\text{dom } f_1 = \{x \in \text{dom } g \mid g(x) \in \text{dom } h\}$

$$h(z) = c_0 + c_1 z + c_2 z^2, z \in (0, +\infty)$$

$$\text{where: } c_0 = \dot{m}_{\text{f},\text{nom}} b_e (a_0 + a_1 n_{sh}^*)$$

$$c_1 = \dot{m}_{\text{f},\text{nom}} b_e (a_2 + a_5 n_{sh}^*)$$

$$c_2 = \dot{m}_{\text{f},\text{nom}} b_e a_4$$

$$g(x) = c_3 - c_4 x, x \in [M_{\text{IM,min}}, M_{\text{IM,max}}]$$

$$\text{where: } c_3 = P_{\text{p,dem}}$$

$$c_4 = 2\pi n_{sh}$$

$z = P_e$ is only meaningful when $z \in [0, 1]$ i.e within the operating envelope of the engine. However, fuel consumption (function h) values are also defined outside this domain, which helps prove its convexity. The following apply:

- g is linear, therefore both convex and concave.
- h is continuous and twice differentiable, with a positive second derivative $\frac{d^2 h}{dz^2} = c_2 = a_4 \dot{m}_{\text{f},\text{nom}}$. As such, it is convex and non-decreasing in \mathbb{R}_{++} .

Since g is both convex and concave, and h is convex and non-decreasing, f_1 is convex.

A.4. Diesel-generator fuel consumption

Following the same procedure, $f_2(x)$ is written as $(h \circ g)(x, y)$. Here $g(x, y)$ refers to the normalised diesel generator's power output, being a function of the induction machine torque and battery power. $h(g(x, y))$ refers to fuel consumption as a function of power output from Eq. (68). Therefore:

$$f_2(x) = (h \circ g)(x, y),$$

with $\text{dom } f_2 = \{(x, y) \in \text{dom } g \mid g(x, y) \in \text{dom } h\}$

$$h(z) = b_{\text{dg}} (a_0 + a_1 z + a_2 z^2), z \in (0, 1]$$

where: $a_i > 0$, $i = 0, 1, 2$ are given by Eq. (68)

$$g(x, y) = c_0 x + c_1 q(x) - y + c_2,$$

$$x \in [M_{\text{im},\min}, M_{\text{im},\max}], y \in [P_{\text{bat},\min}, P_{\text{bat},\max}]$$

$$\text{where: } c_0 = b_{\text{im}} 4\pi n_{\text{sh}}, c_1 = 2b_{\text{im}}, c_2 = P_h b_{\text{im}}$$

$$q(x) = c_{00} + c_{01}x + c_{02}x^2$$

$$\text{with: } \frac{c_{00}}{P_{\text{im},\text{loss nom}}} = (a_{i1}n_{\text{sh}}^* + a_{i3}n_{\text{sh}}^{*2})$$

$$c_{01} = \frac{P_{\text{im},\text{loss nom}}}{M_{\text{im},\text{nom}}} (a_{i2} + a_{i5}n_{\text{sh}}^*)$$

$$c_{02} = P_{\text{im},\text{loss nom}} \frac{a_{i4}}{M_{\text{im},\text{nom}}^2}$$

$a_{ij}, i = 1, 2 \& j = 1, 2...5$ constants

a_{i4} , $i = 1, 2$ & $j = 1, 2...5$ constants

We can show that h is convex and non-decreasing in a similar way. Only proof that $g(x, y)$ is convex is needed and will be presented: g is twice differentiable for $\forall x, y \in \{\text{dom } g | x \neq 0\}$. For $x = 0$, the following apply:

$$\lim_{x \rightarrow 0^-} (g(x, y)) = c_1 c_{00} + c_2 - y$$

$$\lim_{x \rightarrow 0^+} (g(x, y)) = c_1 c_{00} + c_2 - y$$

Since $c_{00} = f(a_{i1}, a_{i3})$ is the same both for motoring and generating conditions, then:

$$\lim_{x \rightarrow 0^-} (g(x, y)) = \lim_{x \rightarrow 0^+} (g(x, y)) \quad \forall y \in \text{dom } g$$

Furthermore:

$$\lim_{\epsilon \rightarrow 0} \left(\frac{g(0 + \epsilon, y) - g(0, y)}{\epsilon} \right) = c_0 + c_{01}$$

$$\lim_{x \rightarrow 0^-} \left(\frac{\partial g(x, y)}{\partial x} \right) = \lim_{x \rightarrow 0^+} \left(\frac{\partial g(x, y)}{\partial x} \right) = c_0 + c_1 c_{01}$$

$$\lim_{\epsilon \rightarrow 0} \left(\frac{\frac{\partial g(0 + \epsilon, y)}{\partial x} - \frac{\partial g(0, y)}{\partial x}}{\epsilon} \right) = 2c_{02}$$

Since $c_{02} = f(a_{i4})$ changes value around $x = 0$, the first derivative of g is not differentiable. Therefore, we will use [Theorem 1](#).

Let $z_1 = (x_1, y_1)$ and $z_2 = (x_2, y_2)$, then:

$$\begin{aligned} g(z_2) &\geq g(z_1) + \nabla^\top g(z_1)(z_2 - z_1) \\ \nabla g(z) &= \begin{bmatrix} \frac{\partial g(z)}{\partial x} \\ \frac{\partial g(z)}{\partial y} \end{bmatrix} = \begin{bmatrix} c_0 + c_1 (c_{01} + 2x c_{02}) \\ -1 \end{bmatrix} \Rightarrow \\ c_0 x_2 + c_1 q(x_2) - y_2 + c_2 &\geq c_0 x_1 + c_1 q(x_1) - y_1 + c_2 + \\ + (c_0 + c_1 (c_{01} + 2x c_{02})) (x_2 - x_1) - (y_2 - y_1) &\Rightarrow \\ \Rightarrow c_1 c_{02} (x_1 - x_2)^2 &\geq 0 \end{aligned}$$

which is true for $\forall x_1, x_2 \in \text{dom } g$, considering:

- $c_1 = 2 > 0$
- $c_{02} = f(a_{i4}) > 0$ for both motoring and generating conditions, since $a_{i4} > 0$, $i = 1, 2$.

As such, g is convex, and since h is both convex and non-decreasing, f_2 is convex.

A.5. Battery equivalent fuel consumption

f_3 is a function of y of the following form:

$$f_3(y) = c_1 \frac{y}{(c_{00} + c_{01}|y| + c_{02}|y|^2)^{\text{sgn}(y)}}, \quad y \in [P_{\text{bat},\min}, P_{\text{bat},\max}]$$

$$\text{where: } c_1 = \eta_{\text{rec}} \frac{s}{Q_{\text{lhv}}}$$

$$c_{00} = a_0$$

$$c_{01} = \frac{a_1}{n_s n_p}$$

$$c_{02} = \frac{a_2}{(n_s n_p)^2}$$

with $a_i, i = 0, 1, 2$ constants

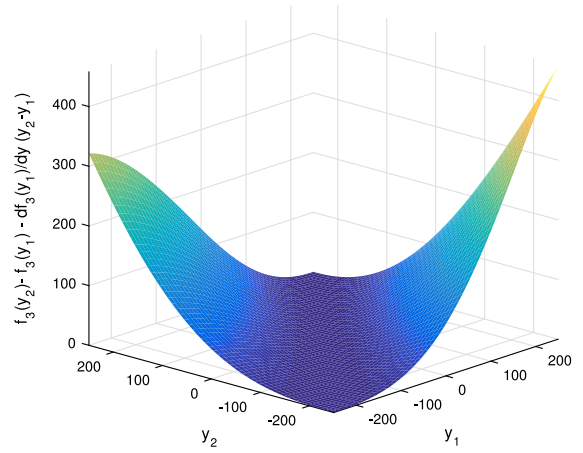


Fig. A.26. Left hand-side of Eq. (A.1).

f_3 is differentiable for $\forall y \in \{\text{dom } f_3 | y \neq 0\}$. For $y = 0$, the following apply:

$$\lim_{y \rightarrow 0^-} (f_3(y)) = \lim_{y \rightarrow 0^+} (f_3(y)) = 0$$

$$\lim_{\epsilon \rightarrow 0^+} \left(\frac{f_3(0 + \epsilon) - f_3(0)}{\epsilon} \right) = \frac{c_1}{c_{00}}$$

$$\lim_{\epsilon \rightarrow 0^-} \left(\frac{f_3(0 + \epsilon) - f_3(0)}{\epsilon} \right) = c_1 c_{00}$$

Since $c_{00} = a_0 = 1$, then:

$$\lim_{\epsilon \rightarrow 0^+} \left(\frac{f_3(0 + \epsilon) - f_3(0)}{\epsilon} \right) = \lim_{\epsilon \rightarrow 0^-} \left(\frac{f_3(0 + \epsilon) - f_3(0)}{\epsilon} \right) = c_1$$

Therefore, f_3 is differentiable for $\forall y \in \text{dom } f_3$, with:

$$\begin{aligned} \frac{\partial f_3}{\partial y} &= \frac{1}{(c_{00} + c_{01}|y| + c_{02}|y|^2)^{\text{sgn}(y)}} - \\ &- y \left(\text{sgn}(y) \frac{c_{01}\text{sgn}(y) + 2c_{02}|y|\text{sgn}(y)}{(c_{00} + c_{01}|y| + c_{02}|y|^2)^{\text{sgn}(y)+1}} \right) \end{aligned}$$

Convexity can be proven using [Theorem 1](#):

$$\begin{aligned} f_3(y_2) &\geq f_3(y_1) + \frac{\partial f_3}{\partial y}(y_1)(y_2 - y_1) \Rightarrow \\ \Rightarrow f_3(y_2) - f_3(y_1) - \frac{\partial f_3}{\partial y}(y_1)(y_2 - y_1) &\geq 0 \end{aligned} \quad (\text{A.1})$$

Due to the complexity of the functions involved, the inequality was not solved analytically. Plotting the left-hand side over the whole range of (y_1, y_2) , shown in [Fig. A.26](#), it can be seen that the inequality holds for $\forall y \in \text{dom } f_3$. Since all f_1, f_2, f_3 are convex, $f(x, y)$, being $m_{f,\text{eqv}}$, is convex as well.

The power to the main Diesel engine is a linear function of the power of the induction machine, therefore it is both convex and concave. The same applies to the constraint for the state of charge of the battery, which is a linear function of the battery power. Therefore, all the constraints of the problem, along with the objective function are convex.

Appendix B. Pontryagin's minimum principle

In the following we will explain why a constant equivalence factor can be considered for this optimal control problem using Pontryagin's Minimum Principle (PMP). PMP redefines the problem in terms of necessary local conditions, expressed by a set of first-order differential equations and an instantaneous minimisation ([Kirk, 2012](#); [Zak, 2003](#)).

The Hamilton–Jacobi–Bellman (HJB) equation, indicates that searching for the optimal control input can be done by minimising the

Hamiltonian:

$$u^*(t) = \underset{u(t) \in \mathcal{U}'}{\operatorname{argmin}} H(t, x(t), u(t), r(t)) \quad (\text{B.1})$$

\mathcal{U} being the set of admissible control values.

From the Hamiltonian we can derive necessary, but not sufficient, conditions for optimality on u and s , as PMP shows:

$$\dot{x}^*(t) = \frac{\partial H}{\partial s} \Big|_{u^*(t)} = f(t, x^*(t), u^*(t)) \quad (\text{B.2})$$

$$\begin{aligned} \dot{s}^*(t) &= -\frac{\partial H}{\partial x} \Big|_{u^*(t)} = -\frac{\partial L}{\partial x}(u^*(t), t) - \\ &- s^*(t) \frac{\partial f}{\partial x}(x^*(t), u^*(t), t) \end{aligned} \quad (\text{B.3})$$

$$H(t, u^*(t), x^*(t), s^*(t)) \leq H(t, u(t), x^*(t), s^*(t)), \quad (\text{B.4})$$

$$\forall u(t) \in U(t), \forall t \in [t_0, t_f] \quad (\text{B.4})$$

$$x(t_0) = x_0, x(t_f) = x_{\text{final}} \quad (\text{B.5})$$

L is the instantaneous cost, state variable is $x = S_{OC}$, and f represents the right hand side of the system dynamic equation. Considering the simple battery model (one constant resistor), the state of charge variation is:

$$\begin{aligned} \dot{x}^*(t) &= \frac{\partial S_{OC}^*}{\partial t} = -\frac{1}{\eta_{\text{bat}}^{\operatorname{sgn}(i_{\text{bat}}(t))}} \frac{i_{\text{bat}}(t)}{Q_{\text{bat,nom}}} = \\ &= -\frac{1}{Q_{\text{bat,nom}} \eta_{\text{bat}}^{\operatorname{sgn}(P_{\text{bat}}^*(t))}} \times \\ &\times \left(\frac{u_{\text{oc}}(x)}{2R} - \sqrt{\left(\frac{u_{\text{oc}}(x)}{2r} \right)^2 - \frac{P_{\text{bat}}^*(t)}{n_s n_p r}} \right) \end{aligned} \quad (\text{B.6})$$

where the open cell voltage u_{oc} and battery efficiency are given by Eqs. (41)–(69), respectively.

Therefore:

$$\begin{aligned} \frac{d\dot{x}^*(t)}{dx} &= \frac{\partial f}{\partial x}(x^*(t), u^*(t), t) = -\frac{1}{Q_{\text{bat,nom}} \eta_{\text{bat}}^{\operatorname{sgn}(P_{\text{bat}}^*(t))}} \times \\ &\times \frac{\partial}{\partial x} \left(\frac{u_{\text{oc}}(x(t))}{2r} - \sqrt{\left(\frac{u_{\text{oc}}(x(t))}{2r} \right)^2 - \frac{P_{\text{bat}}^*(t)}{n_s n_p r}} \right) = \\ &= \frac{4(n_s n_p)^{\sigma_2} P_{\text{bat}}^*(t)}{Q_{\text{bat,nom}}} \times \\ &\times \left(\frac{\nu_4}{2} + x^*(t)v_5 + \frac{\sigma_3}{2} + (v_4 + 2x^*(t)v_5 + \sigma_3 \sigma_1) \frac{\sigma_5}{2\sigma_4} + \frac{\sigma_1}{2} \right) \times \\ &\times \left(a_0 n_s^2 n_p^2 + a_1 n_s n_p P_{\text{bat}}^*(t) + a_2 P_{\text{bat}}^{*2}(t) \right)^{\operatorname{sgn}(P_{\text{bat}}^*(t))} \times \\ &\times \frac{1}{(v_3 + x^*(t)v_4 + \sigma_6 + x^*(t)^2 v_5 + x^*(t)^3 v_6 + \sigma_4)^2} \end{aligned} \quad (\text{B.7})$$

where:

$$\sigma_1 = v_1 v_2 e^{v_2 x}$$

$$\sigma_2 = 2 \operatorname{sgn}(P_B^*(t)) - 1$$

$$\sigma_3 = 3x^2 v_6$$

$$\sigma_4 = \sqrt{\sigma_5^2 - \frac{4 R P_B^*(t)}{n_s n_p}}$$

$$\sigma_5 = v_3 + x v_4 + \sigma_6 + x^2 v_5 + x^3 v_6$$

$$\sigma_6 = v_1 e^{v_2 x}$$

Using Eq. (B.3):

$$\dot{s}^*(t) = -\frac{\partial H}{\partial x} \Big|_{u^*(t)} = -\frac{\partial L}{\partial x} - s^*(t) \frac{\partial f}{\partial x} \Rightarrow \dot{s}^*(t) = -\frac{\partial f}{\partial x} \quad (\text{B.8})$$

The right hand side of Eq. (B.8), is given by Eq. (B.7), and is plotted in Fig. B.27. As can be seen, its variation is relatively small compared to the absolute value of the equivalence factor (the value corresponding to the nominal sfc of the main engines is 2.36). To this end, we can safely assume that:

$$\frac{\dot{s}^*(t)}{s^*(t)} = -\frac{\partial f}{\partial x} \approx 0 \Rightarrow s^*(t) = \text{const} \quad (\text{B.9})$$

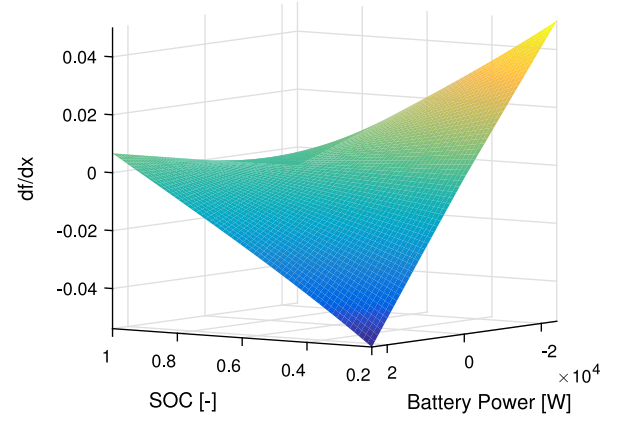


Fig. B.27. Right hand-side of Eq. (B.8).

References

- Ambühl, D., & Guzzella, L. (2009). Predictive reference signal generator for hybrid electric vehicles. *IEEE Transactions on Vehicular Technology*, 58(9), 4730–4740.
- Ambühl, D., Sciarretta, A., Onder, C., Guzzella, L., Sterzing, S., & Mann, K., et al. (2007). A causal operation strategy for hybrid electric vehicles based on optimal control theory. In Proc. 4th symp hybrid vehicles and energy management (pp. 318–331).
- Ambühl, D., Sundstrom, O., Sciarretta, A., & Guzzella, L. (2010). Explicit optimal control policy and its practical application for hybrid electric powertrains. *Control Engineering Practice*, 18(12), 1429–1439.
- Barcellos, R. (2013). The hybrid propulsion system as an alternative for offshore vessels servicing and supporting remote oil field operations. In *Proceedings of the annual offshore technology conference*, vol. 3 (pp. 1622–1631).
- Baumann, B., Rizzoni, G., & Washington, G. (1998). *Intelligent control of hybrid vehicles using neural networks and fuzzy logic*. SAE Technical Papers.
- Bosich, D., & Sulligoi, G. (2013). Voltage control on a refitted luxury yacht using hybrid electric propulsion and LVDC distribution. In *Proc. 8th int. conf. ecological vehicles and renewable energies* (pp. 1–6).
- Breijis, A., & El Aman, E. (2016). Energy management - adapt your engine to every mission. In *Proc 13th INEC* (pp. 1–8).
- Capasso, C., & Veneri, O. (2014). Experimental analysis on the performance of lithium-based batteries for road full electric and hybrid vehicles. *Applied Energy*, 136, 921–930.
- Capasso, C., Veneri, O., Notti, E., Sala, A., Figari, M., & Martelli, M. (2016). Preliminary design of the hybrid propulsion architecture for the research vessel G. Dalaporta. In *Conf. Proc. ESARS-ITEC 2016*.
- Castles, G., Reed, G., Bendre, A., & Pitsch, R. (2009). Economic benefits of hybrid drive propulsion for naval ships. In *Proc. IEEE electric ship technologies symposium* (pp. 515–520).
- Chasse, A., Pognant-Gros, P., & Sciarretta, A. (2009). Online implementation of an optimal supervisory control for a parallel hybrid powertrain. *SAE International Journal of Engines*, 2, 1630–1638.
- Chasse, A., & Sciarretta, A. (2011). Supervisory control of hybrid powertrains: an experimental benchmark of offline optimization and online energy management. *Control Engineering Practice*, 19(11), 1253–1265.
- Chen, S. K., & Flynn, P. F. (1965). Development of a single cylinder compression ignition research engine. In *SAE technical paper of comb. powerpl. and transport. meet*.
- Colonna, V. P., & Van Putten, H. (2007). Dynamic modeling of steam power cycles: part i-Modeling paradigm and validation. *Applied Thermal Engineering*, 27(2), 467–480.
- Dedes, E. (2013). *Investigation of hybrid systems for diesel powered ships* (Ph.D. thesis), University of Southampton.
- Dedes, E., Hudson, D. A., & Turnock, S. R. (2012). Assessing the potential of hybrid energy technology to reduce exhaust emissions from global shipping. *Energy Policy*, 40, 204–218.
- de Groot, D., & van Koperen, R. (2014). Fuel economy: hybrid solutions and beyond. In *Conf. Proc. ITS* (pp. 1–10).
- Delprat, S., Guerra, T. M., & Rimaux, J. (2002). Control strategies for hybrid vehicles: optimal control. In *Proc. IEEE 56th vehicular technology conference*, vol. 3 (pp. 1681–1685).
- Dib, W., Chasse, A., Moulin, P., Sciarretta, A., & Corde, G. (2014). Optimal energy management for an electric vehicle in eco-driving applications. *Control Engineering Practice*, 29, 299–307.
- Doerry, N., Robey, H., Amy, J., & Petry, C. (1996). Powering the future with the integrated power systemtem. *Journal of Naval Engineering*, 267–282.
- Drijver, J. (2013). *Evaluation of transmission losses, heat flows and temperatures of propulsive drive lines* (Master's thesis), Delft, the Netherlands: Delft University of Technology.

- Elbert, P., Ebbesen, S., & Guzzella, L. (2013). Implementation of dynamic programming for n-dimensional optimal control problems with final state constraints. *IEEE Transactions on Control Systems Technology*, 21(3), 924–931.
- Erdinc, O., Vural, B., & Uzunoglu, M. (2009). A dynamic lithium-ion battery model considering the effects of temperature and capacity fading. In *Proc. intern. conf. on clean electrical power* (pp. 383–386).
- Falcao, J., Castro, R., & de Jesus, J. M. F. (2016). Frequency control during transients in offshore wind parks using battery energy storage systems. *Journal of Marine Engineering and Technology*, 15(2), 57–68.
- Flower, J., & Hodge, C. (2014). Stability and transient-behavioural assessment of power-electronics based dc-distribution systems. Part 4: Simple compensation to improve system performance. *Journal of Marine Engineering and Technology*, 13(2), 3–11.
- Formentin, S., Guanetti, J., & Savaresi, S. M. (2016). Least costly energy management for series hybrid electric vehicles. *Control Engineering Practice*, 48, 37–51.
- Gao, L., Liu, S., & Dougal, R. A. (2002). Dynamic lithium-ion battery model for system simulation. *IEEE Transactions on Components and Packaging Technologies*, 25(3), 495–505.
- Geertsma, R., Negenborn, R., Visser, K., & Hopman, J. (2016). Torque control for diesel mechanical and hybrid propulsion for naval vessels. In *Proc. 13th INEC* (pp. 476–92).
- Geertsma, R. D., Negenborn, R. R., Visser, K., & Hopman, J. J. (2017a). Design and control of hybrid power and propulsion systems for smart ships: A review of developments. *Applied Energy*, 194, 30–54.
- Geertsma, R. D., Negenborn, R. R., Visser, K., & Hopman, J. J. (2017b). Pitch control for ships with mechanical and hybrid propulsion: modeling, validation and performance quantification. *Applied Energy*, 206, 1609–1631.
- Geertsma, R. D., Vollbrandt, J., Negenborn, R. R., Visser, K., & Hopman, J. J. (2017). A quantitative comparison of hybrid diesel-electric and gas-turbine-electric propulsion for future frigates. In *Proc. Electric Ship Tech Symp* (pp. 451–458).
- Godjevac, M., Drijver, J., de Vries, L., & Stapersma, D. (2015). Evaluation of losses in maritime gearboxes. *Proceedings of IMechE, Part M: Journal of Engineering for the Maritime Environment*, 1–16.
- Grimmelius, H. T., de Vos, P., Krijgsman, M., & van Deursen, E. (2011). Control of hybrid ship drive systems. In *Proc. 10th conf. computer and its applications in the maritime industry*.
- Guardiola, C., Pla, B., Onori, S., & Rizzoni, G. (2014). Insight into the HEV/PHEV optimal control solution based on a new tuning method. *Control Engineering Practice*, 29, 247–256.
- Guzzella, L., & Onder, C. (2009). *Introduction to modeling and control of internal combustion engine systems*. Berlin, Germany: Springer Science & Business Media.
- Guzzella, L., Sciarretta, A., et al. (2007). *Vehicle propulsion systems* (Vol. 1). Berlin, Germany: Springer.
- Heseltalab, A., & Negenborn, R. R. et al. (2017). Predictive on-board power management for all-electric ships with dc distribution architecture. In *Proc. conf. oceans*.
- Heseltalab, A., Negenborn, R. R., & Lodewijks, G. (2016). Multi-level predictive control for energy management of hybrid ships in the presence of uncertainty and environmental disturbances. *IFAC-PapersOnLine*, 49(3), 90–95.
- Herdzik, J. (2013). Problems of propulsion systems and main engines choice for offshore support vessels. *Zeszyty Naukowe/Akademia Morska W Szczecinie*.
- Herrera, L., Zhang, W., & Wang, J. (2017). Stability analysis and controller design of dc microgrids with constant power loads. *IEEE Transactions on Smart Grid*, 8(2), 881–888.
- Heywood, J. B., et al. (1988). *Internal combustion engine fundamentals* (Vol. 930). New York, USA: McGraw-Hill.
- Hillier, F. S. (2012). *Introduction to operations research*. McGraw-Hill Education.
- Hofman, T., & Janssen, N. H. J. (2017). Integrated design optimization of the transmission system and vehicle control for electric vehicles. *IFAC-PapersOnLine*, 50(1), 10072–10077.
- Hu, X., Li, S., & Peng, H. (2012). A comparative study of equivalent circuit models for Li-ion batteries. *Journal of Power Sources*, 198, 359–367.
- International Maritime Organization, (2014). *Third IMO GHG study: prevention of air pollution from ships. Tech. rep.* London, UK: International Maritime Organization.
- Jager, B. D., Keulen, T. V., & Kessels, J. T. B. A. (2013). *Optimal control of hybrid vehicles*. Springer.
- Jamel, M., Rahman, A. A., & Shamsuddin, A. (2013). Advances in the integration of solar thermal energy with conventional and non-conventional power plants. *Renewable and Sustainable Energy Reviews*, 20(C), 71–81.
- Johannesson, L., Murgovski, N., Jonasson, E., Hellgren, J., & Egardt, B. (2015). Predictive energy management of hybrid long-haul trucks. *Control Engineering Practice*, 41, 83–97.
- Kalikatzarakis, M. (2017). *Energy management for hybrid tugs* (Master's thesis), Delft, the Netherlands: Delft University of Technology.
- Karlsen, A. T. (2012). *On modeling of a ship propulsion system for control purposes* (Master's thesis), Trondheim, Norway: Norwegian University of Science and Technology.
- Kermani, S., Delprat, S., Guerra, T.-M., Trigui, R., & Jeanneret, B. (2012). Predictive energy management for hybrid vehicle. *Control Engineering Practice*, 20(4), 408–420.
- Kessels, J. T., Koot, M. W., Van Den Bosch, P. P., & Kok, D. B. (2008). Online energy management for hybrid electric vehicles. *IEEE Transactions on Vehicular Technology*, 57(6), 3428–3440.
- Khoury, G., Ghosn, R., Khatounian, F., Fadel, M., & Tientcheu, M. (2016). Including core losses in induction motors dynamic model. In *Proc. 3rd intern. conf. REDEC* (pp. 526–531).
- Kim, N., Cha, S., & Peng, H. (2011). Optimal control of hybrid electric vehicles based on Pontryagin's minimum principle. *IEEE Transactions on Control Systems Technology*, 19(5), 1279–1287.
- Kirk, D. (2012). *Optimal control theory: an introduction*. New York, USA: Prentice Hall.
- Koot, M., Kessels, J. T., De Jager, B., Heemels, W., Van den Bosch, P., & Steinbuch, M. (2005). Energy management strategies for vehicular electric power systems. *IEEE Transactions on Vehicular Technology*, 54(3), 771–782.
- Kuiper, G. (1992). *The wageningen propeller series*. MARIN.
- Kumar, Y., Ringenberg, J., Depuru, S. S., Devabhaktuni, V. K., Lee, J. W., Nikolaidis, E., et al. (2016). Wind energy: Trends and enabling technologies. *Renewable and Sustainable Energy Reviews*, 53(C), 209–224.
- Maamria, D., Sciarretta, A., Chaplais, F., & Petit, N. (2017). Online energy management system (EMS) including engine and catalyst temperatures for a parallel HEV. *IFAC-PapersOnLine*, 50(1), 8913–8920.
- Murgovski, N., Johannesson, L., Sjoberg, J., & Egardt, B. (2012). Component sizing of a plug-in hybrid electric powertrain via convex optimization. *Mechatronics*, 22, 106–120.
- Musardo, C., Rizzoni, G., Guezenne, Y., & Staccia, B. (2005). A-ECMS: An adaptive algorithm for hybrid electric vehicle energy management. *European Journal of Control*, 11(4–5), 509–524.
- Nuesch, T., Wang, M., Isenegger, P., Onder, C. H., Steiner, R., Macri-Lassus, P., et al. (2014). Optimal energy management for a diesel hybrid electric vehicle considering transient PM and quasi-static NOx emissions. *Control Engineering Practice*, 29, 266–276.
- Ong, C. M. (1998). *Dynamic simulation of electric machinery: using matlab/simulink* (Vol. 5). Prentice Hall Publishing House.
- Onori, S., & Serrao, L. (2011). On adaptive-ecms strategies for hybrid electric vehicles. In *Proc. intern. sc. conf. on hybrid and electric vehicles* (pp. 6–7).
- Onori, S., Serrao, L., & Rizzoni, G. (2016). *Hybrid electric vehicles: Energy management strategies*. Berlin, Germany: Springer.
- Ovrum, E., & Bergh, T. (2015). Modelling lithium-ion battery hybrid ship crane operation. *Applied Energy*, 152, 162–172.
- Paganelli, G. (1999). *Conception et commande d'une chaîne de traction pour véhicule hybride parallèle thermique et électrique* (Ph.D. thesis), Valenciennes: Université de Valenciennes.
- Paganelli, G., Delprat, S., Guerra, T. M., Rimaux, J., & Santin, J. J. (2002). Equivalent consumption minimization strategy for parallel hybrid powertrains. In *Conf. proc. 55th IEEE vehicular technology conference* (pp. 2076–2081).
- Paganelli, G., Guerra, T., Delprat, S., Santin, J., Delhom, M., & Combes, E. (2000). Simulation and assessment of power control strategies for a parallel hybrid car. *Proceedings of IMechE, Part D: Journal of Automobile Engineering*, 214(7), 705–717.
- Patel, M. R. (2012). *Shipboard propulsion, power electronics, and ocean energy*. CRC Press.
- Ross, R., Stapersma, D., & Bosklopper, J. (2010). Fuel efficiency of diesel, electric and superconductive propulsion systems. In *Proc. 10th INEC*.
- Salman, M., Schouten, N. J., & Kheir, N. A. (2000). Control strategies for parallel hybrid vehicles. In *Proc. IEEE American control conference*, vol. 1(6) (pp. 524–528).
- Sciarretta, A., Back, M., & Guzzella, L. (2004). Optimal control of parallel hybrid electric vehicles. *IEEE Transactions on Control Systems Technology*, 12(3), 352–363.
- Sciarretta, A., & Guzzella, L. (2007). Control of hybrid electric vehicles. *IEEE Control Systems*, 27(2), 60–70.
- Sciarretta, A., Serrao, L., Dewangan, P., Tona, P., Bergshoeff, E., Bordons, C., et al. (2014). A control benchmark on the energy management of a plug-in hybrid electric vehicle. *Control Engineering Practice*, 29, 287–298.
- Sciberras, E., Bashar, Z., David, A., et al. (2015). Electric auxiliary propulsion for improved fuel efficiency and reduced emissions. *Proceedings of IMechE, Part M: Journal of Engineering for the Maritime Environment*, 229(1), 36–44.
- Sciberras, E., & Norman, R. (2012). Multi-objective design of a hybrid propulsion system for marine vessels. *IET Electrical Systems in Transportation*, 2(3), 148–157.
- Serrao, L., Hubert, C. J., & Rizzoni, G. (2007). Dynamic modeling of heavy-duty hybrid electric vehicles. In *Proc. ASME 2007 intern. mech. engin. congress and expo*, vol. 16 (pp. 121–128).
- Serrao, L., Sciarretta, A., Grondin, O., Chasse, A., Creff, Y., Di Domenico, D., et al. (2013). Open issues in supervisory control of hybrid electric vehicles: A unified approach using optimal control methods. *Oil and Gas Science and Technology*, 68(1), 23–33.
- Shaheen, S. A., & Lipman, T. E. (2007). Reducing greenhouse emissions and fuel consumption: Sustainable approaches for surface transportation. *IATSS Research*, 31(1), 6–20.
- Shi, W., Grimmelius, H. T., & Stapersma, D. (2010). Analysis of ship propulsion system behaviour and the impact on fuel consumption. *International Shipbuilding Progress*, 57, 35–64.
- Shiraishi, K., Minami, S., Kobayashi, K., et al. (2013). Development of a hybrid tugboat propulsion system. *MTZ Industrial*, 3(2), 36–43.
- Silvas, E., Hofman, T., Murgovski, N., Etman, L. F. P., & Steinbuch, M. (2017). Review of optimization strategies for system-level design in hybrid electric vehicles. *IEEE Transactions on Vehicular Technology*, 66(1), 57–70.
- Simmonds, O. J. (2014). DC: Is it the alternative choice for naval power distribution?. *Journal of Marine Engineering and Technology*, 13(3), 37–43.
- Sivertsson, M., & Eriksson, L. (2015). Design and evaluation of energy management using map-based ECMS for the PHEV benchmark. *Oil and Gas Science and Technology*, 70(1), 195–211.

- Stapersma, D. (2010a). *Diesel engines volume 1 - performance analysis* (8th ed.). Delft, the Netherlands: Delft University of Technology.
- Stapersma, D. (2010b). *Diesel engines volume 2 -turbocharging* (8th ed.). Delft, the Netherlands: Delft University of Technology.
- Stapersma, D. (2010c). *Diesel engines volume 3 - combustion* (8th ed.). Delft, the Netherlands: Delft University of Technology.
- Stapersma, D. (2010d). *Diesel engines volume 4 - emissions and heat transfer* (8th ed.). Delft, the Netherlands: Delft University of Technology.
- Stopford, M. (2008). *Maritime economics* (3rd ed.). London, UK: Routledge.
- Sulligoi, G., Castellan, S., Aizza, M., Bosich, D., Piva, L., & Lipardi, G. (2012). Active front-end for shaft power generation and voltage control in FREMM frigates integrated power system: Modeling and validation. In *Proc. intern. symp. SPEEDAM* (pp. 452–457).
- Sundstrom, O., Ambuhl, D., & Guzzella, L. (2010). On implementation of dynamic programming for optimal control problems with final state constraints. *Oil and Gas Science and Technology*, 65(1), 91–102.
- Sundstrom, O., & Guzzella, L. (2009). A generic dynamic programming matlab function. In Proc. IEEE control appl. (CCA) and intell. control (pp. 1625–1630).
- Taljegard, M., Brynolf, S., Grahn, M., Andersson, K., & Johnson, H. (2014). Cost-effective choices of marine fuels in a carbon-constrained world: results from a global energy model. *Environmental Science and Technology*, 48, 12986–12993.
- Tian, Y., Xia, B., Wang, M., Sun, W., & Xu, Z. (2014). Comparison study on two model-based adaptive algorithms for SOC estimation of lithium-ion batteries in electric vehicles. *Energies*, 7(12), 8446–8464.
- Trzynadlowski, A. M. (2001). *Control of induction motors*. San Diego, California, USA: Academic press.
- Van Biert, L., Godjevac, M., Visser, K., & Aravind, P. V. (2016). A review of fuel cell systems for maritime applications. *Journal of Power Sources*, 327, 345–364.
- van Koperen, R. (2009). *Conceptual design of an environmentally friendly harbour tug* (Master's thesis), Delft, the Netherlands: Delft University of Technology.
- van Loon, P. T., & van Zon, P. (2016). From operational profile to hybrid propulsion. In *Proceedings of the 24th international HISWA symposium on Yacht design and Yacht construction* (pp. 1–13).
- Veneri, O., Migliardini, F., Capasso, C., & Corbo, P. (2012). Overview of electric propulsion and generation architectures for naval applications. In *Conf. Proc. ESARS-ITEC 2012*.
- Volker, T. (2013). Hybrid propulsion concepts on ships. *Zeszyty Naukowe Akademii Morskiej W Gdyni*, 79, 66–76.
- Vu, T. L. (2015). Power management for electric tugboats through operating load estimation. *IEEE Transactions on Control Systems Technology*, 23(6), 2375–2382.
- Vu, T. L., et al. (2014). Optimal power management for electric tugboats with unknown load demand. In *Proc. IEEE American control conference* (pp. 1578–1583).
- Waag, W., Fleischer, C., & Sauer, D. U. (2014). Critical review of the methods for monitoring of lithium-ion batteries in electric and hybrid vehicles. *Journal of Power Sources*, 258, 321–339.
- Whitelegg, I., Bucknall, R. W. G., & Thorp, B. T. (2015). On electric warship power system performance when meeting the energy requirements of electromagnetic railguns. *Journal of Marine Engineering and Technology*, 14(2), 85–102.
- Wijsmuller M., H. T. (2007). Optimization of the propulsion arrangement in emergency towing vessels. *Ship and Boat International*, 34–37.
- Won, J.-S., Langari, R., & Ehsani, M. (2005). An energy management and charge sustaining strategy for a parallel hybrid vehicle with cvt. *IEEE Transactions on Control Systems Technology*, 13(2), 313–320.
- Xu, L., Nueller, C. D., Li, J., Ouyang, M., & Hu, Z. (2015). Multi-objective component sizing based on optimal energy management strategy of fuel cell electric vehicles. *Applied Energy*, 157, 664–674.
- Yuan, L. C. W., Tjahjowidodo, T., & Lee, G. S. G., et al. (2016). Equivalent consumption minimization strategy for hybrid all-electric tugboats to optimize fuel savings. In *2016 American control conference* (pp. 6803–6808).
- Zahedi, B., & Norum, L. E. (2013). Modeling and simulation of all-electric ships with low-voltage DC hybrid power systems. *IEEE Transactions on Power Electronics*, 28(10), 4525–4537.
- Zahedi, B., Norum, L. E., & Ludvigsen, K. B. (2014). Optimized efficiency of all-electric ships by dc hybrid power systems. *Journal of Power Sources*, 255, 341–354.
- Zak, S. H. (2003). *Systems and control*. Oxford University Press.
- Zhan, K., Gao, H., Chen, H., & Lin, Z. (2015). Optimal retrofitting of a hybrid propulsion system using nsga-ii algorithm for trailing suction hopper dredger. In *Proc. IEEE electric ship technologies symposium* (pp. 201–206).
- Zheng, F., Xing, Y., Jiang, J., Sun, B., Kim, J., & Pecht, M. (2016). Influence of different open circuit voltage tests on state of charge online estimation for lithium-ion batteries. *Applied Energy*, 183, 513–525.